Geosci. Model Dev. Discuss., 7, 8649–8701, 2014
www.geosci-model-dev-discuss.net/7/8649/2014/
doi:10.5194/gmdd-7-8649-2014

Geoscientific Model Development Discussions
Open Access

A multi-layer land surface energy budget model for implicit coupling with global atmospheric simulations

J. Ryder[1], J. Polcher[2], P. Peylin[1], C. Ottlé[1], Y. Chen[1], E. van Gorsel[3], V. Haverd[3], M. J. McGrath[1], K. Naudts[1], J. Otto[1,*], A. Valade[1], and S. Luyssaert[1]

[1]Laboratoire des Sciences du Climat et de l'Environnement (LSCE-IPSL, CEA-CNRS-UVSQ), Orme des Merisiers, 91191 Gif-sur-Yvette, France
[2]Laboratoire de Météorologie Dynamique (LMD, CNRS), Ecole Polytechnique, 91128 Palaiseau, France
[3]CSIRO Oceans and Atmosphere Flagship, 2 Wilf Crane Cr., Yarralumla, ACT 2600, Australia
[*]now at: Climate Service Center 2.0, Helmholtz-Zentrum Geesthacht, Hamburg, Germany

Received: 9 October 2014 – Accepted: 30 October 2014 – Published: 8 December 2014

Correspondence to: J. Ryder (jryder@lsce.ipsl.fr)

Published by Copernicus Publications on behalf of the European Geosciences Union.

Abstract

In Earth system modelling, a description of the energy budget of the vegetated surface layer is fundamental as it determines the meteorological conditions in the planetary boundary layer and as such contributes to the atmospheric conditions and its circulation. The energy budget in most Earth system models has long been based on a "big-leaf approach", with averaging schemes that represent in-canopy processes. Such models have difficulties in reproducing consistently the energy balance in field observations. We here outline a newly developed numerical model for energy budget simulation, as a component of the land surface model ORCHIDEE-CAN (Organising Carbon and Hydrology In Dynamic Ecosystems – CANopy). This new model implements techniques from single-site canopy models in a practical way. It includes representation of in-canopy transport, a multilayer longwave radiation budget, height-specific calculation of aerodynamic and stomatal conductance, and interaction with the bare soil flux within the canopy space. Significantly, it avoids iterations over the height of tha canopy and so maintains implicit coupling to the atmospheric model LMDz. As a first test, the model is evaluated against data from both an intensive measurement campaign and longer term eddy covariance measurements for the intensively studied Eucalyptus stand at Tumbarumba, Australia. The model performs well in replicating both diurnal and annual cycles of fluxes, as well as the gradients of sensible heat fluxes. However, the model overestimates sensible heat flux against an underestimate of the radiation budget. Improved performance is expected through the implementation of a more detailed calculation of stand albedo and a more up-to-date stomatal conductance calculation.

1 Introduction

Earth system models are the most advanced tools to predict future climate (Bonan, 2008). These models represent the interactions between the atmosphere and the surface beneath, with the surface formalized as a combination of open oceans, sea-ice

GMDD
7, 8649–8701, 2014

and land. For land, a description of the energy budget of the vegetated surface layer is fundamental as it determines the meteorological conditions in the planetary boundary layer and as such contributes to the atmospheric conditions and its circulation.

The vegetated surface layer of the Earth is subject to incoming and outgoing fluxes of energy, namely atmospheric sensible heat (H, $\mathrm{W\,m^{-2}}$), latent heat (LE, $\mathrm{W\,m^{-2}}$), shortwave radiation from the sun (R_{SW}, $\mathrm{W\,m^{-2}}$), longwave radiation (R_{LW}, $\mathrm{W\,m^{-2}}$) emitted from other radiative sources such as clouds and atmospheric compounds and soil heat exchange with the subsurface (G, $\mathrm{W\,m^{-2}}$). The sum of these fluxes is equal to the amount of energy that is stored or released from the surface layer over a given time period Δt (s). So, for a surface of overall heat capacity C_p ($\mathrm{J\,K^{-1}\,m^{-2}}$) the temperature change over time, ΔT, is described as:

$$C_p \frac{\Delta T}{\Delta t} = H + \mathrm{LE} + R_{\mathrm{LW}} + R_{\mathrm{SW}} + G. \quad (1)$$

One key concept in modelling the energy budget of the surface Eq. (1) is the way in which the surface layer is defined. In many cases the surface layer describes both the soil cover and the vegetation above it as a uniform block. Such an approach is known as a "big leaf model", so called because the entirety of the volume of the trees or crops and the understorey, as well as the surface layer, are simulated in one entity, to produce fluxes parameterised from field measurements. In the model under study, named ORCHIDEE-CAN (Organising Carbon and Hydrology In Dynamic Ecosystems – CANopy) (Naudts et al., 2014), the land surface is effectively simulated as an "infinitesimal surface layer" – a conceptual construct of zero thickness. As demonstrated in the original paper describing this model, such an approach, whilst reducing the canopy to simple components, was nevertheless able to simulate surface fluxes to an acceptable degree of accuracy for the sites that were evaluated as the original SECHIBA (Schematic of Hydrological Exchange at the Biosphere to Atmosphere Interface) model (Schulz et al., 2001) and later as a component of the original ORCHIDEE model (Krinner et al., 2005), precursor to ORCHIDEE-CAN.

GMDD
7, 8649–8701, 2014

The proof that existing land to surface simulations may now be inadequate comes from inter-comparison studies, such as Pitman et al. (2009), which evaluated the response of such models to land use change scenarios. That study found a marked lack of consistency between the models, an observation they attributed to a combination of the varying implementation of LCC (Land Cover Change) maps, the representation of crop phenology, the parameterisation of albedo and the representation of evapotranspiration for different land cover types. Regarding the latter two issues, the models they examined did not simulate in a transparent, comparable manner the changes in albedo and evapotranspiration as a result of changes in vegetation cover, such as from forest to cropland. It was not possible to provide a definitive description of the response of latent heat flux to land cover change across the seven models under study, because there was substantial difference in the mechanisms which describe the evaporative response to the net radiation change across the conducted simulations.

Furthermore, the latent and sensible heat fluxes from off-line land surface models were reported to depend very strongly on the process-based parameterisation, even when forced with the same micro-meteorological data (Jiménez et al., 2011).The structure of land surface models, it has been suggested (Schlosser and Gao, 2010), may be more important than the input data in simulating evapotranspiration. Hence, improvements to the soil-surface–atmosphere interaction (Seneviratne et al., 2010), and to the hydrology (Balsamo et al., 2009), are considered essential for better simulating evapotranspiration. We can therefore assert that refinements in the numerical schemes of land surface models represent a logical approach to the further constraint of global energy and water budgets.

Large scale validation, therefore, has revealed that the “big leaf approach” has difficulties in reproducing fluxes of sensible and latent heat (Jiménez et al., 2011; Pitman et al., 2009; de Noblet-Ducoudré et al., 2012) for a wide range of vegetated surfaces. This lack of modelling capability is thought to be due to the “big leaf approach” not representing the vertical canopy structures in detail and thus not simulating factors such as radiation partition, separation of height classes, turbulent transport within the

GMDD
7, 8649–8701, 2014

vegetation and canopy–atmosphere interactions – all of which are crucial factors in the improved determination of sensible and latent heat flux estimates (Baldocchi and Wilson, 2001; Ogée et al., 2003; Bonan et al., 2014), as well as the presence of an understorey, or mixed canopies, as is proposed by Dolman (1993). Furthermore, a model that is able to determine the temperatures of elements throughout the canopy profile will provide for a more useful comparison with remote sensing devices, for which the "remotely sensed surface temperature" also depends on the viewing angle (Zhao and Qualls, 2005, 2006).

This gap in modelling capability provides the motivation for developing and testing a new, multi-layer, version of the energy budget simulation based on Eq. (1). A multi-layer approach is expected to model more subtle but important differences in the energy budget in relation to multi-layer vegetation types such as forests, grasses and crops. Through the simulation of more than one canopy layer, the model could simulate the energy budget of different plant types in two or more layers such as found in savannah, grassland, wood species and agro-forestry systems (Verhoef and Allen, 2000; Saux-Picart et al., 2009)

2 Model requirements

Several alternative approaches to the big leaf model have been developed. These alternatives share the search for a more detailed representation of some of the interactions between the heat and radiation fluxes and the surface layer. Following Baldocchi and Wilson (2001), the range and evolution of such models includes:

1. the big-leaf model (e.g. Penman and Schofield, 1951)
2. the big-leaf with dual sources (e.g. Shuttleworth and Wallace, 1985)
3. two layer models which split the canopy from the soil layer (e.g. Dolman, 1993; Verhoef and Allen, 2000; Yamazaki et al., 1992)

GMDD
7, 8649–8701, 2014

4. three layer models, which split the canopy from the soil layer, and simulate the canopy as a seperate understorey and overstorey (e.g. Saux-Picart et al., 2009)

5. 1-D multi-layer models (e.g. Baldocchi and Wilson, 2001)

6. 3-D models that consist of an array of plants and canopy elements (e.g. Sinoquet et al., 2001).

For coupling to an atmospheric model (see below), and thus running at a global scale, simplicity, robustness, generality and computational speed need to be balanced. We therefore propose a 1-D multi-layer model combined with a statistical description of the 3-D canopy. We aim for a multi-layer canopy model that:

- simulates processes that are sufficiently well understood at a canopy level such that they can be parameterised at the global scale through (semi-)mechanistic, rather than empirical, techniques. Examples of such processes are the description of stomatal conductance (Ball et al., 1987; Medlyn et al., 2011), and the partition of radiation in transmitted, reflected and absorbed radiation at different canopy levels (Pinty et al., 2006; McGrath et al., 2014).
- Simulates the exposure of each section of the canopy, and the soil layer, to both shortwave and longwave radiation. At the same time the model should also simulate in-canopy gradients, separating between soil-surface–atmosphere and vegetation–atmosphere interactions.
- Simulates non-standard canopy set-ups, for instance combining different species in the same vertical structure, e.g. herbaceous structures under trees, as explored by Dolman (1993); Verhoef and Allen (2000); Saux-Picart et al. (2009).
- Describes directly the interaction between the soil surface and the sub-canopy using an assigned soil resistance rather than a soil-canopy amalgamation.

GMDD
7, 8649–8701, 2014

– Is flexible, that is to say sufficiently stable to be run over fifty layers or over just two, i.e. the soil-surface and the canopy.

– Avoids introducing interactions that would require iterative solutions.

Where the first five requirements relate to the process description of the multi-layer model, the last requirement is imposed by the need to couple ORCHIDEE to an atmospheric model. Generally, coupling an implicit scheme will be more stable than an explicit scheme, which means that it can be run over longer timesteps. Furthermore, the approach is robust: for example, if there is an instability in the atmospheric model, it will tend to be dampened in subsequent timesteps, rather than diverge progressively. For this work, the model needs to be designed to be run over time steps as long as 30 min in order to match the timesteps of the IPSL atmospheric model, called LMDz (Laboratoire de Météorologie Dynamique Zoom model; Hourdin et al., 2006), to which it is coupled, and so to conserve processing time. However, the mathematics of an implicit scheme have to be linearised and is thus by necessity rigidly and carefully designed. As discussed in Polcher et al. (1998) and subsequently in Best et al. (2004), the use of implicit coupling was widespread in models when the land surface was a simple bucket model, but as the land surface schemes have increased in complexity, explicit schemes have, for most models, been used instead, because complex explicit schemes are more straightforward to derive than implicit schemes. As they demonstrate, there is nevertheless a framework for simulating all land-surface fluxes and processes (up to a height of, say, 50 m, so including above canopy physics) in a tiled "non-bucket" surface model coupled, using an implicit scheme, to an atmospheric model.

3 Model description

We here summarise the key components of a new implicit multi-layer energy budget model. The important innovation, compared to existing multi-layer canopy models that work at the local scale (e.g. Baldocchi, 1988; Ogée et al., 2003), is that we will solve the

GMDD
7, 8649–8701, 2014

problems implicitly – i.e. all variables are described in terms of the "next" timestep. The notation used here is listed in full in Table 1, and is chosen to complement the description of the LMDz coupling scheme, as is described in Polcher et al. (1998). A complete version of the derivation of the numerical scheme is provided in the Supplement.

We propose to regard the canopy as a network of potentials and resistances, as shown in Fig. 1, a variation of which was first proposed in Waggoner et al. (1969). At each level in the network we have the state variable potentials: the temperature of the atmosphere at that level, the atmospheric humidity and the leaf level temperature. We include in the network fluxes of latent heat and sensible heat between the leaves at each level and the atmosphere, and vertically between each canopy level. The soil surface interacts with the lowest canopy level, and uppermost canopy level interacts with the atmosphere. We also consider the absorption and reflection of radiation by each vegetation layer and by the surface (SW and LW) and emission of radiation (LW only). This represents the "classic" multi-layer canopy model formulation, with a network of resistances that stimulate the connection between the soil surface temperature and humidity, and fluxes passing through the canopy to the atmosphere.

The analogy is the "circuit diagram" approach, for which T_a and q_a represent the atmospheric "potentials" of temperature and specific humidity at different heights and H and LE are the sensible and latent heat fluxes that act as "currents" for these potentials. At each level within the vegetation, T_a and q_a interact with the leaf level temperature and humidity T_L and q_L through the resistances R_i (for aerodynamic resistance) and R_i' (for stomatal resistance). The change in leaf level temperature is determined by the energy balance at each level.

The modelling approach formalises the following constraints and assumptions.

3.1 Leaf vapour pressure assumption

We assume that the air within leaf level cavities is completely saturated. This means that the vapour pressure of the leaf can be calculated as the saturated vapour pressure at that leaf temperature (Monteith and Unsworth, 2008). Therefore the change

GMDD
7, 8649–8701, 2014

in pressure within the leaf is assumed proportional to the difference in temperature between the present timestep and the next one, multiplied by the rate of change in saturated pressure against temperature.

$$q_0 \equiv q_{\mathrm{L},i}^{t+1} = q_{\mathrm{sat}}^{T_{\mathrm{L},i}^t} + \left.\frac{\delta q_{\mathrm{sat}}}{\delta T}\right|_{T_{\mathrm{L},i}^t} \left(T_{\mathrm{L},i}^{t+1} - T_{\mathrm{L},i}^t\right) \tag{2}$$

$$= \left.\frac{\delta q_{\mathrm{sat}}}{\delta T}\right|_{T_{\mathrm{L},i}^t} (T_{\mathrm{L},i}^{t+1}) + \left(q_{\mathrm{sat}}^{T_{\mathrm{L},i}^t} - T_{\mathrm{L},i}^t \left.\frac{\delta q_{\mathrm{sat}}}{\delta T}\right|_{T_{\mathrm{L},i}^t}\right) \tag{3}$$

$$= \alpha_i T_{\mathrm{L},i}^{t+1} + \beta_i \tag{4}$$

where α_i and β_i are regarded as constants for each particular level and timestep, so $\alpha_i = \left.\frac{\delta q_{\mathrm{sat}}}{\delta T}\right|_{T_{\mathrm{L},i}^t}$ and $\beta_i = \left(q_{\mathrm{sat}}^{T_{\mathrm{L},i}^t} - T_{\mathrm{L},i}^t \left.\frac{\delta q_{\mathrm{sat}}}{\delta T}\right|_{T_{\mathrm{L},i}^t}\right)$

To find a solution we still need to find an expression for the terms $q_{\mathrm{sat}}^{T_{\mathrm{L},i}^t}$ and $\left.\frac{\delta q_{\mathrm{sat}}}{\delta T}\right|_{T_{\mathrm{L},i}^t}$ in α_i and β_i above.

Using the empirical approximation of Tetens (e.g., Monteith and Unsworth, 2008, their Sect. 2.1) and the specific humidity vapour pressure relationship we can describe the saturation vapour pressure to within 1 Pa up to a temperature of about 35 °C.

$$e_{\mathrm{sat}}(T) = e_{\mathrm{sat}}(T^*) \exp[A(T - T^*)/(T - T')] \tag{5}$$

where $A = 17.27$, $T^* = 273\,\mathrm{K}$, $e_{\mathrm{sat}}(T^*) = 0.611\,\mathrm{kPa}$, $T' = 36\,\mathrm{K}$.

Specific humidity is related to vapour pressure by the relationship: (e.g., Monteith and Unsworth, 2008, their Sect. 2.1):

$$q = \frac{\left(\frac{M_{\mathrm{W}}}{M_{\mathrm{A}}}\right) e}{(p - e) + \left(\frac{M_{\mathrm{W}}}{M_{\mathrm{A}}}\right) e} \tag{6}$$

GMDD
7, 8649–8701, 2014

where q = specific humidity ($\mathrm{kg\,kg^{-1}}$), e = vapour pressure (kPa), $(M_\mathrm{W}/M_\mathrm{A})$ = (ratio of molecular weight of water to air) = 0.622, and p = atmospheric pressure (kPa)

To find $q_{\mathrm{sat}}^{T_{\mathrm{L},i}^t}$, we substitute $e_{\mathrm{sat}}(T_\mathrm{L})$ derived from Eq. (5) for e in Eq. (6):

$$q_{\mathrm{sat}}^{T_\mathrm{L}} = \frac{\left(\frac{M_\mathrm{W}}{M_\mathrm{A}}\right) e_{\mathrm{sat}}(T_\mathrm{L})}{(p - e_{\mathrm{sat}}(T_\mathrm{L})) + \left(\frac{M_\mathrm{W}}{M_\mathrm{A}}\right) e_{\mathrm{sat}}(T_\mathrm{L})} \tag{7}$$

To calculate $\frac{\delta q_{\mathrm{sat}}}{\delta T}|_{T_{\mathrm{L},i}^t}$, we use the expression for the saturated humidity curve against temperature (as derived using the method of Monteith and Unsworth, 2008):

$$q_{\mathrm{sat}}^{T_{\mathrm{L},i}^t} = q_0 e^{-\lambda M_\mathrm{W}/RT} \tag{8}$$

The derivative of this expression is:

$$\left.\frac{\delta q_{\mathrm{sat}}}{\delta T}\right|_{T_{\mathrm{L},i}^t} = \frac{\lambda M_\mathrm{W} q_{\mathrm{sat}}(T)}{R(T_{\mathrm{L},i}^t)^2} \tag{9}$$

So $\frac{\delta q_{\mathrm{sat}}}{\delta T}|_{T_{\mathrm{L},i}^t}$ can be determined by substitution of the expression for $q_{\mathrm{sat}}(T_\mathrm{L})$ from Eq. (7) into Eq. (9):

$$\frac{\delta q_{\mathrm{sat}}}{\delta T}|_{T_{\mathrm{L},i}^t} = \frac{\lambda M_\mathrm{W}}{R(T_{\mathrm{L},i}^t)^2} \frac{\left(\frac{M_\mathrm{W}}{M_\mathrm{A}}\right) e_{\mathrm{sat}}(T_\mathrm{L})}{(p - e_{\mathrm{sat}}(T_\mathrm{L})) + \left(\frac{M_\mathrm{W}}{M_\mathrm{A}}\right) e_{\mathrm{sat}}(T_\mathrm{L})} \approx \frac{\lambda M_\mathrm{W}}{R(T_{\mathrm{L},i}^t)^2} \frac{\left(\frac{M_\mathrm{W}}{M_\mathrm{A}}\right) e_{\mathrm{sat}}(T_\mathrm{L})}{p} \tag{10}$$

Thus the specific humidity of the leaf follows a relationship to the leaf temperature that is described by a saturation curve.

GMDD
7, 8649–8701, 2014

3.2 Derivation of the leaf layer resistances (R_i and R'_i)

The variables R_i and R'_i represent the leaf layer resistance to the sensible and latent heat flux, respectively. R_i is calculated based upon the leaf boundary layer resistance, and is described according to the following expression from Baldocchi (1988):

$$R_b(z) = \frac{l}{\mathrm{d}f(z)D_z Sh(z)} \tag{11}$$

where R_b denotes the boundary layer resistance ($= R_i$), l is the characteristic length of leaves, D_s is the molecular diffusivity of the entity in question and Sh is the Sherwood number, as calculated in Baldocchi (1988). R'_i is the stomatal resistance of the leaf that is calculated using the method of Lohammer et al. (1980), after Jarvis (1976), but there is potential for a more up-to-date parameterisation such as that of Medlyn et al. (2011).

3.3 The leaf energy balance equation for each layer

For vegetation, we assume the energy balance is satisfied for each layer. We extend Eq. (1) in order to describe a vegetation layer of volume ΔV_i, area ΔA_i and thickness Δh_i:

$$\Delta V_i \theta_i \rho_v \frac{\delta T_{L,i}}{\delta t} = (H_i + \mathrm{LE}_i + R_{SW,i} + R_{LW,i})\Delta A_i \tag{12}$$

All terms are defined in Table 1. The heat capacity of each vegetation layer (Θ_i) is assumed equal to that of water, and is modulated according to the Leaf Area Density ($\mathrm{m}^2\,\mathrm{m}^{-3}$) at that level. Since the fluxes in the model are described per square metre, ΔA_i may be represented by the Plant Area Density ($\mathrm{PAD}, \mathrm{m}^2\,\mathrm{m}^{-3}$) for that layer, where "plant" denotes leaves, stems, grasses or any other vegetation included in Leaf Area Index (LAI) measurements. Note that LAI, that has units of $\mathrm{m}^2\,\mathrm{m}^{-2}$, is a value that describes the integration over the whole of the canopy profile of PAD (which is applied

GMDD
7, 8649–8701, 2014

per metre of height, hence the dimension $m^2\,m^{-3}$). Canopy layers that do not contain foliage may be accounted for at a level by assigning that $R_i = R'_i = \infty$ for that level (i.e. an open circuit).

Rewriting Eq. (8) in terms of the state variables and resistances that are shown in Fig. 1 means that R_i is the resistance to sensible heat flux and R'_i the resistance to latent heat flux. Dividing both sides of the equation by ΔV_i, the volume of the vegetation layer (equal to Δh_i multiplied by ΔA_i), expresses the sensible and latent heat fluxes between the leaf and the atmosphere respectively as:

$$\text{(a)}\ \ \theta_i \rho_v \frac{\delta T_{L,i}}{\delta t} = \left(\Theta_{p,\,a} \rho_a \frac{(T_{L,i} - T_{a,i})}{R_i} + \lambda \rho_a \frac{(q_{L,i} - q_{a,i})}{R'_i} + R_{SW,i} + R_{LW(tot),i} \right) \left(\frac{1}{\Delta h_i} \right) \tag{13}$$

n.b. this is the first of three key equations that are labelled (a), (b) or (c) on the left hand side, throughout.

3.3.1 Vertical transport within a column

The transport equation between each of the vegetation layer segments may be described as:

$$\frac{\delta(\rho\chi)}{\delta t} + \mathrm{div}(\rho\chi \boldsymbol{u}) = \mathrm{div}(\Gamma \mathrm{grad}(\chi)) + S_\chi \tag{14}$$

where div is the operator that calculates the divergence of the vector field, χ is the property under question, ρ is the fluid density, $\boldsymbol{u}$ is the horizontal wind speed vector (assumed negligible here), S_χ is the concentration for the property in question and Γ is a parameter that will in this case be the diffusion coefficient $k(z)$.

To derive from this expression the conservation of scalars equation, as might be applied to vertical air columns, we proceed according to the Finite Volume Method, as

GMDD
7, 8649–8701, 2014

used in the FRAME (Fine Resolution Atmospheric Multi-pollutant Exchange; Singles et al., 1998) model and as detailed in Vieno (2006) for that model. A description of the Finite Volume Method is in Jacobson (2005). The final equation is specific to a 1-D model, and so does not include a term of the influence of horizontal wind. The resulting expression is sufficiently flexible to allow for variation in the height of each layer, but we preserve vegetation layers of equal height here for simplicity:

$$\frac{\delta\chi}{\delta t}\Delta V = k(z)\frac{\delta d^2\chi}{\delta z^2}\Delta A + S(z)\Delta V \tag{15}$$

$$= \frac{\delta}{\delta z}\left(k(z)\frac{\delta\chi}{\delta z}\right)\Delta A + S(z)\Delta V \tag{16}$$

$$= \frac{\delta}{\delta z}\left(F(z)\right)\Delta A + S(z)\Delta V \tag{17}$$

where F is the vertical flux density, z represents coordinates in the vertical and x coordinates in the streamwise direction. χ may represent the concentration of any constituent that may include water vapour or heat, but also gas or aerosol phase concentration of particular species. S represents the source density of that constituent (in this case the fluxes of latent and sensible heat from the vegetation layer), and the transport $k(z)$ term represents the vertical transport between each layer.

In the equation above, we substitute the flux-gradient relationship according to the expression:

$$F(z) = -k(z)\frac{\delta\chi}{\delta z} \tag{18}$$

This approach allows future applications to include a supplementary term to simulate emissions or deposition of gas or aerosol based species using the same technique.

The transport term, per level i in the vertically discretised form, k_i is calculated using the 1-D second-order closure model of Massman and Weil (1999), which makes use of the LAI profile of the stand. Their model provides profiles σ_w, the SD in vertical velocity

GMDD
7, 8649–8701, 2014

and T_L, the Lagrangian timescale within the canopy. The eddy diffusivity $k_i(z)$ is then derived in the far-field using the expressions from Raupach (1989b):

$$k_i = \sigma_{w,i}^2 T_{L,i} \tag{19}$$

However, the simulation of near field transport in canopies is more complex, and requires ideally a Lagrangian solution (Raupach, 1989a). As that is not directly possible in this implicit solution, we instead adopt a method developed by Makar et al. (1999) (and later Stroud et al., 2005, and Wolfe and Thornton, 2010) for the transport of chemistry species in canopies for which a "near-field" correction term R is introduced to the far-field solution, and is expressed as follows:

$$R(\tau) = \frac{(1 - e^{-\tau/T_L})(\tau/T_L - 1)^{3/2}}{(\tau/T_L - 1 + e^{-\tau/T_L})^{3/2}} \tag{20}$$

where τ represents the time since emission for a theoretical near-field diffusing cloud of a canopy source, as defined in Raupach (1989a) which, unlike for the far-field, acts as point source travelling uniformly in all directions. There is thus a modified expression for k_i, with R acting effectively as a tuning coefficient:

$$k_i^* = R(\tau)\sigma_{w,i}^2 T_{L,i} \tag{21}$$

The necessity to account for the near-field transport effect in canopies, and in particular open canopies, remains a question under discussion (McNaughton and van den Hurk, 1995; Wolfe and Thornton, 2010).

3.3.2 Fluxes of sensible and latent heat between each atmospheric layer

We re-write the scalar conservation equation (Eq. 15, above), as applied to canopies, as a pair of expressions for the fluxes of sensible and latent heat (so, comparing with

GMDD
7, 8649–8701, 2014

Eq. (15), $\chi \equiv T$ or q, $F \equiv H$ or LE and $S \equiv$ (the source sensible or latent heat flux at each vegetation layer)).

Neither the sensible or latent heat flux profile is constant over the height of the canopy. The rate of change of $T_{a,i}$ (the temperature of the atmosphere surrounding the leaf at level i) and $q_{a,i}$ (the specific humidity of the atmosphere surrounding the leaf at level i) are proportional to the rate of change of the respective fluxes with height and the source of heat fluxes from the leaf at that level:

$$\text{(b)}\ \Theta_{p,\,a}\rho_a \frac{\delta T_{a,i}}{\delta t}\Delta V_i = -\frac{\delta H_{a,i}}{\delta z}\Delta A_i + \left(\frac{T_{L,i} - T_{a,i}}{R_i}\right)\left(\frac{\Theta_{p,\,a}\rho_a}{\Delta h_i}\right)\Delta V_i \tag{22}$$

now we assume the flux-gradient relation and so write Eq. (18) according to sensible heat flux at level i, $H_{a,i}$:

$$H_{a,i} = -(\rho_a \Theta_{p,\,a}) k_i \frac{\delta T_{a,i}}{\delta z} \tag{23}$$

which is substituted in Eq. (22)

$$\text{(b)}\ \frac{\delta T_{a,i}}{\delta t}\Delta V_i = k_i \frac{\delta^2 T_{a,i}}{\delta z^2}\Delta A_i + \left(\frac{T_{L,i} - T_{a,i}}{R_i}\right)\left(\frac{1}{\Delta h_i}\right)\Delta V_i \tag{24}$$

and in exactly the same format for the expression for latent heat flux at level i, $\text{LE}_{a,i}$:

$$(\text{LE})_{a,i} = -(\lambda \rho_a) k_i \frac{\delta q_{a,i}}{\delta z} \tag{25}$$

GMDD
7, 8649–8701, 2014

which is, again, substituted in Eq. (22):

$$\text{(c)}\ \lambda\rho_{\mathrm{a}}\frac{\delta q_{\mathrm{a},i}}{\delta t}\Delta V_i = -\frac{\delta(\mathrm{LE})_{\mathrm{a},i}}{\delta z}\Delta A_i + \left(\frac{q_{\mathrm{L},i} - q_{\mathrm{a},i}}{R'_i}\right)\left(\frac{\lambda\rho_{\mathrm{a}}}{\Delta h_i}\right)\Delta V_i \tag{26}$$

$$= -\frac{\delta(\mathrm{LE})_{\mathrm{a},i}}{\delta z}\Delta A_i + \left(\frac{(\alpha T_{\mathrm{L},i} + \beta_i) - q_{\mathrm{a},i}}{R'_i}\right)\left(\frac{\lambda\rho_{\mathrm{a}}}{\Delta h_i}\right)\Delta V_i \tag{27}$$

$$\text{(c)}\ \frac{\delta q_{\mathrm{a},i}}{\delta t}\Delta V_i = k_i\frac{\delta^2 q_{\mathrm{a},i}}{\delta z^2}\Delta A_i + \left(\frac{(\alpha T_{\mathrm{L},i} + \beta_i) - q_{\mathrm{a},i}}{R'_i}\right)\left(\frac{1}{\Delta h_i}\Delta V_i\right) \tag{28}$$

We have now defined the three key equations in the model:

- Equation (a) balances the energy budget at each vegetation level.
- Equation (b) balances heat fluxes vertically between each vegetation level and "horizontally" between each vegetation level and the surrounding atmosphere.
- Equation (c) balances humidity fluxes in the same sense as for Eq. (b).

The equations must be solved simultaneously, whilst at the same time satisfying the limitations of an implicit scheme.

3.3.3 Write equations in implicit format

The difference between explicit and implicit schemes is that an explicit scheme will calculate each value of the variable (i.e. temperature and humidity) at the next time step entirely in terms of values from the present time step. An implicit scheme requires the solution of equations that couple together values at the next time step. The basic differencing scheme for implicit equations is described by Richtmyer and Morton (1967). In that work, they introduce the method with an example equation:

$$u^{t+1} = B(\Delta t, \Delta x, \Delta y)u_t \tag{29}$$

GMDD
7, 8649–8701, 2014

where B denotes a linear finite difference operator, Δt, Δx, Δy are increments in the respective co-ordinates and u_t, u_{t+1} are the solutions at respectively steps "t" and "$t+1$".

It is therefore assumed that B depends on the size of the increments Δt, Δx, Δy and that, once known, it may be used to derive u_{n+1} from u_n. So if B can be determined we can use this relationship to calculate the next value in the sequence. However, we necessarily need to know the initial value in the sequence (i.e. u_0). This means that it is an "initial value problem". Now, the equivalent of Eq. (18), in the context of a column model, such as LMDz, takes the form:

$$X_l = C_l^X + D_l^X X_{l-1} \tag{30}$$

This describes the state variable X (for example temperature) at level l, in relation to the value at level $l-1$. C_l^X and D_l^X are coupling coefficients that are derived in that scheme. In this particular example, the value of W_l at time t is defined in terms of X_{l-1} at the same timestep.

To maintain the implicit coupling between the atmospheric model (i.e. LMDz) and the land surface model (i.e. ORCHIDEE) we need to express the relationships that are outlined above in terms of a linear relationship between the "present" timestep t and the "next" timestep $t+1$. We therefore re-write Eqs. (a)–(c) in implicit form (i.e. in terms of the "next" timestep, which is $t+1$), as below:

implicit form of the energy balance equation: we substitute the expressions for leaf level vapour pressure Eq. (4) to the energy balance equation Eq. (13), which we rewrite in implicit form:

$$\text{(a)}\ \ \theta_i \rho_\mathrm{v} \frac{(T_{\mathrm{L},i}^{t+1} - T_{\mathrm{L},i}^{t})}{\Delta t} = \left(\frac{1}{\Delta h_i}\right)\left(\Theta_{p,\,\mathrm{a}}\rho_\mathrm{a}\frac{(T_{\mathrm{L},i}^{t+1} - T_{\mathrm{a},i}^{t+1})}{R_i} + \lambda\rho_\mathrm{a}\frac{(\alpha_i T_{\mathrm{L},i}^{t+1} + \beta_i - q_{\mathrm{a},i}^{t+1})}{R_i'}\right. \tag{31}$$
$$\left. + \eta_1 R_\mathrm{LW}^\mathrm{down} + \eta_2 T_{\mathrm{L},i}^{t+1} + \eta_3 + \eta_4 R_\mathrm{SW}^\mathrm{down}\right)$$

GMDD
7, 8649–8701, 2014

Implicit form of the sensible heat flux equation

We difference Eq. (24) according to the finite volume method Eq. (15), and divide by ΔV_i:

$$\text{(b)}\ \frac{T_{\mathrm{a},i}^{t+1} - T_{\mathrm{a},i}^{t}}{\Delta t} = k_i \left(\frac{\left(T_{\mathrm{a},i+1}^{t+1} - T_{\mathrm{a},i}^{t+1}\right)}{\Delta z_i \Delta h_i} \right) - k_{i-1} \left(\frac{\left(T_{\mathrm{a},i}^{t+1} - T_{\mathrm{a},i-1}^{t+1}\right)}{\Delta z_{i-1} \Delta h_i} \right) + \left(\frac{1}{\Delta h_i} \right) \frac{\left(T_{\mathrm{L},i}^{t+1} - T_{\mathrm{a},i}^{t+1}\right)}{R_i} \quad (32)$$

Implicit form of the latent heat flux equation

We difference Eq. (28) according to the finite volume method Eq. (15), and divide by ΔV_i:

$$\text{(c)}\ \frac{q_{\mathrm{a},i}^{t+1} - q_{\mathrm{a},i}^{t}}{\Delta t} = k_i \left(\frac{\left(q_{\mathrm{a},i+1}^{t+1} - q_{\mathrm{a},i}^{t+1}\right)}{\Delta z_i \Delta h_i} \right) - k_{i-1} \left(\frac{\left(q_{\mathrm{a},i}^{t+1} - q_{\mathrm{a},i-1}^{t+1}\right)}{\Delta z_{i-1} \Delta h_i} \right) + \left(\frac{1}{\Delta h_i} \right) \frac{\left(\alpha_i T_{\mathrm{L},i}^{t+1} + \beta_i - q_{\mathrm{a},i}^{t+1}\right)}{R'_i} \quad (33)$$

These equations are solved by assuming a solution of a particular form and finding the coefficients that are introduced in terms of the coefficients of the layer above. This is "solution by induction".

With respect to Eq. (32), we wish to express $T_{\mathrm{a},i}^{t+1}$ in terms of values further down the column, to allow the equation to solved by "moving up" the column, as in Richtmyer and Morton (1967).

GMDD
7, 8649–8701, 2014

In order to solve by implicit means, we make the assumption (later to be proved by induction) that:

$$\text{(i)}\ T_{\mathrm{a},i}^{t+1} = A_{T,i} T_{\mathrm{a},i-1}^{t+1} + B_{T,i} + C_{T,i} T_{\mathrm{L},i}^{t+1} + D_{T,i} q_{\mathrm{a},i-1}^{t+1} \tag{34}$$

$$\text{(ii)}\ q_{\mathrm{a},i}^{t+1} = A_{q,i} q_{\mathrm{a},i-1}^{t+1} + B_{q,i} + C_{q,i} T_{\mathrm{L},i}^{t+1} + D_{q,i} T_{\mathrm{a},i-1}^{t+1} \tag{35}$$

We then also re-write these expressions in terms of the values of the next level:

$$\text{(i)}\ T_{\mathrm{a},i+1}^{t+1} = A_{T,i+1} T_{\mathrm{a},i}^{t+1} + B_{T,i+1} + C_{T,i+1} T_{\mathrm{L},i+1}^{t+1} + D_{T,i+1} q_{\mathrm{a},i}^{t+1} \tag{36}$$

$$\text{(ii)}\ q_{\mathrm{a},i+1}^{t+1} = A_{q,i+1} q_{\mathrm{a},i}^{t+1} + B_{q,i+1} + C_{q,i+1} T_{\mathrm{L},i+1}^{t+1} + D_{q,i+1} T_{\mathrm{a},i}^{t+1} \tag{37}$$

where $A_{T,i}$, $B_{T,i}$, $C_{T,i}$, $D_{T,i}$, $A_{q,i}$, $B_{q,i}$, $C_{q,i}$ and $D_{q,i}$ are constants for that particular level and timestep and are, as yet, unknown, but will be derived. We thus substitute Eqs. (34) and (36) into Eq. (32) to eliminate T_{t+1}. Symmetrically, we substitute Eqs. (35) and (37) into Eq. (33) to eliminate q_{t+1}.

For the vegetation layer, we conduct a similar procedure, in which the leaf level temperature is described as follows (where E_i, F_i and G_i are known assumed constants for the level and timestep in question):

$$\text{(iii)}\ T_{\mathrm{L},i}^{t+1} = E_i q_{\mathrm{a},i-1}^{t+1} + F_i T_{\mathrm{a},i-1}^{t+1} + G_i \tag{38}$$

Now the coefficients $A_{T,i}$, $B_{T,i}$, $C_{T,i}$, $D_{T,i}$, $A_{q,i}$, $B_{q,i}$, $C_{q,i}$ and $D_{q,i}$ can be described in terms of the coefficients from the level above and the potentials (i.e. T and q) at the previous timestep, which we can in turn determine by means of the boundary conditions. So we have a set of coefficients that may be determined for each time-step, and we have the means to determine T_S (and q_S via the saturation assumption). We thus have a process to calculate the temperature and humidity profiles for each timestep by systematically calculating each of the coefficients from the top of the column (the "downwards sweep") then calculating the "initial value" (the surface temperature and

GMDD
7, 8649–8701, 2014

humidity) and finally calculating each T_a, q_a and T_L by working up the column (the "upwards sweep"). The term $T_{L,i}^{t+1}$ can also be described in terms of the variables at the level below by $T_{L,i+1}^{t+1}$ using Eq. (iii) and its terms E_i, F_i and G_i.

3.4 The boundary conditions

3.4.1 The upper boundary conditions

In stand-alone simulations, the top level variables $A_{T,n}$, $C_{T,n}$, $D_{T,n}$ and $A_{q,n}$, $C_{q,n}$, $D_{q,n}$, are set to zero and $B_{T,n}$ and $B_{q,n}$ set to the input temperature and specific humidity, respectively, for the relevant time step (as in Best et al., 2004) In coupled simulations, $A_{T,n}$, $B_{T,n}$ and $B_{q,n}$, $C_{q,n}$ are taken from the respective values at lowest level of the atmospheric model. Table 2 summarises the boundary conditions for both the coupled and un-coupled simulations.

3.4.2 The lower boundary condition

We need to solve the lowest level transport equations separately, using an approach which accounts for the additional effects of radiation emitted, absorbed and reflected from the vegetation layers:

$$T_S^{t+1} = \frac{T_S^t + \frac{\Delta t}{\theta_0}\left(\eta_{1,S} R_{LW}^{down} + \eta_{3,S} + \eta_{4,S} R_{SW}^{down} + \xi_1 + \xi_3\right) - J_{soil}}{\left(1 - \frac{\Delta t}{\theta_0}(\xi_2 + \xi_4 + \eta_{2,S})\right)} \quad (39)$$

where $\eta_{1,S}$, $\eta_{2,S}$, $\eta_{3,S}$ and $\eta_{4,S}$ are components of the radiation scheme (refer to Sect. S2.9.1 of the Supplement), and ξ_1, ξ_2, ξ_3 and ξ_4 are components of the surface flux (refer to Sect. S3.2 of the Supplement).

GMDD
7, 8649–8701, 2014

3.5 The radiation scheme

A partially implicit longwave radiation scheme was developed for the model, however, the combination of explicit and implicit terms in this scheme resulted in a slight imbalance in the radiation budget. In order to completely conserve energy, we instead make use of an alternative approach – the Longwave Radiation Transfer Matrix (LRTM) (Gu, 1988; Gu et al., 1999).

This approach separates the calculation of the radiation distribution completely from the implicit expression. Instead a single source term for the longwave radiation is added at each level. This means that the distribution of radiation refers to the present time step, rather than the next. However it accounts for a higher order of reflections from adjacent levels than the single order that is assumed in the alternative process.

4 Model set up and simulations

4.1 Selected site and observations

Given the desired capability of the multi-layer model to simulate complex within canopy interactions, we selected a test site with an open canopy. This is because open canopies may be expected to be more complex in terms of their interactions with the overlying atmosphere. In addition, long-term data measurements of the atmospheric fluxes had to be available in order to validate the performance of the model across years and seasons, and within canopy measurements were required in order to validate the capacity of the model to simulate within canopy fluxes. One site that fullfiled these requirements was the long-term measurement site at Tumbarumba in south-eastern inland Australia (35.6° S, 148.2° E, elevation ~ 1200 m) which is part of the global Fluxnet measurement program (Baldocchi et al., 2001). The measurement site is a *Eucalyptus Delegatensis* canopy, a temperate evergreen species, of tall height ~ 40 m. With an LAI of ~ 2.4, the canopy is described as “moderately open”. (Ozflux, 2013)

GMDD
7, 8649–8701, 2014

4.2 Forcing and model comparison data

As a test of stability over a long term run, the model was forced (i.e. run "off-line", independently from the atmospheric model) using above-canopy measurements. The forcing data that was used in this simulation was derived from the long term Fluxnet measurements for the years 2002 to 2007, specifically above-canopy measurements of longwave and shortwave radiation, temperature, humidity, windspeed, rainfall and snowfall. The first four years of data, from 2002 to 2005, were used as a spin-up to charge the soil to its typical water content for the main simulation. The biomass from the spin-up was overwritten by the observed leaf biomass to impose the observed LAI profile. Soil carbon is not required in this study, which justify the short spin-up time. The years 2006 and 2007 were then used as the main part of the run. Although the shortwave radiation measurements are measured in the two components, the longwave radiation measurements are not. As a consequence, the outgoing longwave was calculated using the recorded above canopy temperature and assuming the Stefan–Boltzmann law with an emissivity factor of 0.96 (a standard technique for estimating this variable, e.g. Park et al., 2008). This value is then subtracted from the net radiation, together with the two shortwave components, to obtain an estimation of the downwelling longwave radiation with which to force the model.

For the validation of the within canopy processes more detailed measurement data was required. For the same site there exists data from an intensive campaign of measurements made during November 2006 (Austral summer), described by Haverd et al. (2009). Within the canopy, profiles of temperature and potential temperature were recorded over the 30 day period and, for a number of days (7–14 November), sonic anemometers were used to measure windspeed and sensible heat flux in the vertical profile at eight heights as well. Measurements were also made over the thirty day period of the soil heatflux and the soil water content. These within-canopy data were used for validation of the modelled output but the same above-canopy long-term data (i.e. the Fluxnet data) were used in the forcing file in all cases. No further measurements

GMDD
7, 8649–8701, 2014

were collected specifically for this publication. The measurement data (i.e. the data both from the one month intensive campaign and the long term Fluxnet measurements at the same site Ozflux, 2013) were prepared as an ORCHIDEE forcing file, according to the criteria for gap-filling missing data (Vuichard and Papale, 2014).

4.3 Model set-up

The multi-layer module that is described in this paper only calculates the energy budget. Its code was therefore integrated in the enhanced model ORCHIDEE-CAN, and relies on that larger model for input-output operations of drivers and simulations, as well as the calculation of soil hydrology, soil heat fluxes and photosynthesis (see Table 3 for other input). A more detailed description of how these processes are implemented in ORCHIDEE-CAN is provided in Naudts et al. (2014).

For testing the performance of the multi-layer model, rather than ORCHIDEE-CAN, the most basic options where chosen whenever possible: (1) stomatal conductance was calculated as a function of radiation (Jarvis, 1976) rather than the default approach in ORCHIDEE-CAN that follows Ball et al. (1987) and calculates stomatal conductance as a function of net photosynthesis, relative humidity and CO_2 concentration, (2) the two way multi-layer albedo scheme that is the default for ORCHIDEE-CAN was replaced by an exponential extinction of light as a function of LAI with increasing canopy depth, (3) although the ORCHIDEE-CAN model is capable of simulating the canopy vegetation structure dynamically, a LAD profile was prescribed in these tests, in order to obtain a simulation as close as possible to the observed conditions. LAD is an estimate of the sum of the surface area of all leaves growing on a given land area (e.g. per m^2) over a metre of height. It is effectively LAI (which is expressed as m^2 of leaf per unit square over an entire canopy height) recalculated per unit metre, and thus has units $m^2\,m^{-3}$. As there were no LAD profiles available for the field site at the time of measurement, data from Lovell et al. (2012) for the "Tumbatower" profile, as depicted in Fig. 3 of that publication, were used. The profile was scaled according to the measured site LAI of 2.4, resulting in the profile shown in Fig. 2. As no gap-forming or

GMDD
7, 8649–8701, 2014

stand replacing disturbances have been recorded at the site, the vertical distribution of foliage was assumed unchanged over the period between the different measurement campaigns.

5 Results

The sign convention used here makes all upward fluxes positive (so a positive sensible or latent heat flux from the surface cools the ground). Likewise a negative radiation flux towards the surface warms the ground.

Although the aim of this study is to check the performance of our multi-layer energy budget model against site-level observations, it should be noted that site-level energy fluxes come with their own limitations that result in a so-called closure gap. The closure gap is reflected in a mismatch between the net radiation and the fluxes of latent, sensible and soil heat. For the observations used in this study, the closure gap was $\sim 37\,\mathrm{W\,m^{-2}}$ (7.5 % of total fluxes) during the day and $4\,\mathrm{W\,m^{-2}}$ (4.6 %) during the night. By design, the energy budget model conserves energy, hence, overestimates or underestimates by the model of individual fluxes by 20 %, which is the mean imbalance at Fluxnet sites (Wilson et al., 2002) and could be due to shortcomings in the observations. Underestimation of the data and mismatches exceeding the closure gap are very likely indicate a shortcoming in the model. At a fundamental level, energy budget models distribute the net radiation between sensible, latent and soil heat fluxes. Evaluation of these component fluxes becomes only meaningful when the model reproduces the net radiation (Fig. 3). Note that through its dependency on leaf temperature the calculation of the longwave component of net radiation depends on the sensible, latent and soil heat fluxes. Taken as a whole, there is a good correlation between the observation-driven and model-driven net longwave radiation ($r^2 = 0.87$). However, when the data are separated into nighttime and daytime a clear cycle is revealed for which the model overestimates daytime radiation and underestimates radiation at night. This descrepancy is likely a result of actual daytime heat storage in the soil being underestimated

GMDD
7, 8649–8701, 2014

in the model, an aspect which the model may accommodate by improved parameterisation.

In terms of the current parameterisation, and for the site under study, the annual cycles for both sensible and latent heat are well simulated (Fig. 4a and c). In addition, no clear systematic bias was observed between summer and winter (Fig. 4b and d). But, as shown, there is an overall systematic bias of $-14.8\,W\,m^{-2}$ for sensible heat and $18.5\,W\,m^{-2}$ for latent heat flux, when averaged over the whole year. Such a bias represents $\sim 28\,\%$ of sensible heat and $\sim 27\,\%$ of latent heat fluxes.

The analysis proceeded by further increasing the temporal resolution and testing the capacity of the model to reproduce diurnal flux cycles. The model overestimates the diurnal peak in sensible heat flux, whilst the latent heat flux is underestimated by a smaller magnitude (Fig. 5b). The diurnal pattern of the model biases persists in all four seasons (Supplement Fig. S1a–d). We see that the maximum mean discrepancy between measured and modelled sensible heat flux is an overestimate of roughly $90\,W\,m^{-2}$ (Fig. 5b) and an underestimate of the latent heat flux by $40\,W\,m^{-2}$ (Fig. 5d). Over the course of the year, the difference is largest in the autumn and smallest in the summer (Fig. S2a–d). However, from the net radiation (i.e. the sum of downwelling minus upwelling for longwave and shortwave), we can see that there is a discrepancy between measured and modelled that acts to offset in part the discrepancy observed in the flux plots (Fig. 5a–f). This suggests that with a better parametrisation of factors within the canopy such as albedo (the impact through the shortwave radiation) and stomatal and aerodynamic resistances (which impact the partitioning between the fluxes), the model can likely be parameterised to more closely match observation.

Long-term measurements from above the forest and data from a short intensive field campaign were jointly used to evaluate model performance at different levels within the canopy. For reference, Fig. S3 summarises the downwelling longwave and shortwave radiation measured over this period. As was the case for the annual cycle, the sinusoidal cycles resulting from the diurnal pattern in solar angle are well matched (Fig. 6a–d). Sensible heat flux was measured below and above the canopy and the

GMDD
7, 8649–8701, 2014

model was able to simulate this gradient (Fig. 6a and c). Latent heat flux at an equivalent height of 2 m was not recorded (Fig. 6d). However, the match in magnitude of the measured data is not accurately simulated hour by hour (Fig. 6e).

Using the current parameters, there is a discrepancy between the measured and the modelled temperature gradients within the canopy (Fig. 7). It should be noted that the mean values are strongly determined by a few extreme hours. As such the model is capable of simulating the majority of the time steps but fails to reproduce the more extreme observations. During the daytime, the strong positive gradient in the measured output is only partly reflected in the modelled slopes. At nighttime, there is a clear negative gradient for the measured data, whereas the modelled temperature profile is almost completely uniform. However a temperature profile more closely matched to the measurements (Fig. 8) was achieved through forcing the eddy-diffusivity coefficients by a factor (K_z) of 0.2 (nighttime) and 0.6 (daytime, as determined by the presence of SW radiation) within the canopy. The above canopy fluxes for these two simulations were however almost identical (not shown). Forcing the eddy-diffusivity coefficients to better match the observations demonstrated that the observed mismatch is most likely due to the current parameterisation rather than a numerical limitation of the model.

The version of the model used in these tests is composed of 50 levels, to provide a high resolution simulation and a test of the stability of the scheme. However, a canopy simulation of such detail is likely overly complex for a canopy model that is to be coupled to an atmospheric simulation, in terms of additional run time required, and is probably unnecessary. To provide an evaluation of the difference in fluxes that were predicted by a model of lower resolution, the same tests were conducted with the model composed of 25, 10, 2 and a single vegetation level (note that in all cases the vegetation levels are simulated separately from the surface soil, so the single vegetation model is a two-layer canopy model in the sense that the two levels are the canopy and the soil layer cf., Dolman, 1993). When taken in the context of the annual simulations for the 50-layer case (Fig. 5), these tests show that the difference is slight between the 50-layer and 25-layer case, and between the 50-layer and 10-layer case for both sensible and latent

GMDD
7, 8649–8701, 2014

heat (Fig. 9). In all cases the mean hourly difference over the whole year is always less than 54 $W m^{-2}$ per flux (~ 3 % of the 50 level mean). For the two vegetation layer model the mean hourly difference is always less than 20 $W m^{-2}$ per flux (~ 10 % approx.) and for the one layer vegetation model (with the soil surface modelled separately), the mean hourly difference is always less than 55 $W m^{-2}$ per flux (~ 30 % approx). Figure 10 presents the average RMS error for each day of the year (shown as a rolling average).

6 Discussion

The proposed model is able to simulate fluxes of sensible and latent heat above the canopy over a long term period, as has shown by simulation of conditions at a Fluxnet site on a long term, annual scale (Figs. 4 and 5), and over a concentrated, week-long period (Fig. 6). Although these figures show a discrepancy between measured and modelled fluxes, we see from Fig. 5 that the modelled overestimate of sensible heat flux is offset by an underestimation of latent heat flux and of net radiation. It is likely therefore that this discrepancy can be reduced by an improved simulation of canopy albedo at each level (which determines the distribution and reflection of shortwave radiation over the modelled canopy), and refinements to the calculation of vegetation aerodynamic and stomatal resistances (which affects the split between sensible and latent heat from each modelled layer). In the study of land–atmosphere interactions, the multi-layer model functions to a standard comparable to single-layer models.

The innovation of this model is the capacity to simulate the behaviour of fluxes within the canopy, and the separation of the soil-level temperature from the temperature of the vegetation levels. Uniquely for a canopy model, this is achieved without iterations, as the mathematics have been derived to use the same implicit coupling technique as the existing surface–atmosphere coupling applied in ORCHIDEE/LMDz (Polcher et al., 1998; Best et al., 2004), but now over the height of the canopy. This also means that the model is scalable without impacting heavily on runtimes. For large scale applications,

GMDD
7, 8649–8701, 2014

performance within the canopy must be further constrained through comparison with intensive in-canopy field campaigns from diverse ecosystems.

6.1 Simulation of aerodynamic resistance

In this study, the aerodynamic coefficient that is used in single-layer models was replaced by an eddy diffusivity profile, the purpose of which is two-fold. Firstly, to develop a transport coefficient that is based on the vertical canopy profile and secondly, to more accurately represent the in-canopy gradients of temperature and specific humidity. In this way, it was hoped to contribute to a model that can better allow for such features as vertical canopy gaps (i.e. trunk space between a well separated under and overstorey), horizontal gaps, transport and chemistry between different sections of the canopy, tree growth and the mix of different kinds of vegetation in the same surface layer simulation (e.g. Dolman, 1993). To be able to do this, a height based transport closure model was used to simulate within canopy transport.

A transport closure model contrasts the existing approach within ORCHIDEE, as is used in single layer models. In that approach, aerodynamic interaction between the land surface and the atmosphere is parametrised by the atmospheric resistance R_a and the architectural resistance R_0. R_a is typically calculated through consideration of the roughness height of the canopy (i.e. small for flat surfaces, large for uneven tall surfaces) which in turn is parameterised in surface layer models by canopy height (e.g., LSCE/IPSL, 2012) (however, LAI can display a better correlation with roughness length (a critical parameter) than it does to canopy height, Beringer et al., 2005). In parameterising the roughness length in terms of canopy height alone, no account is made for the clumping of trees, the density of the forest or the phenological changes in stand profile (other than the height) as the stand grows. Some of these changes are compensated for in R_0, the structural coefficient that is unique to each PFT grouping, but does not allow for more subtle effects. To be able to satisfactorily explore such results in a modelling study requires an accurate parametrisation of within-canopy transport.

GMDD
7, 8649–8701, 2014

In this study, canopy transport is parametrised by K-theory, applying the closure model of Massman and Weil (1999) to derive the in-canopy turbulence statistics, based both on the LAI profile and the canopy height. The simulation produces a good estimation of above-canopy fluxes, but the differences between day- and night-time profiles are not well described using the original parametrisation (Fig. 7). This means that the model overestimates the nighttime canopy transport, as compared to the daytime simulation.

Looking more broadly, studies of chemical species transport have demonstrated that K-theory, sometimes constrained by a scaling factor, remains a reasonable approximation for above-canopy fluxes, even if the within-canopy gradients are not entirely correct (Gao et al., 1989; Dolman and Wallace, 1991; Makar et al., 1999; Wolfe and Thornton, 2010). The justification for such a scaling factor seems to vary in terms of the form of the canopy structure, likely related to canopy openness (McNaughton and van den Hurk, 1995; Stroud et al., 2005). Here, too, we find that a scaling factor is necessary to match the gradient fluxes though the scaling factor required varies according to the time of day. During the nighttime (Fig. 8a and d), the measurements show a general positive temperature gradient (as defined from the soil surface moving upwards), which could be replicated through the use of an eddy coefficient factor of 0.2. During the daytime (Fig. 8b and c), the negative gradient can be replicated most closely with an eddy-coefficient factor of 0.6. Parametrisation of models, against the growing amount of detailed canopy measurement campaigns will help to clarify the issue. For a completely satisfactory resolution of this issue, it will be necessary to derive a method to reformulate the method of Raupach (1989a, b) in an implicit form, which lies outside the realm of this paper.

6.2 Simulation of energy partition throughout canopy and soil surface

Trees in a spruce forest have been reported to account for 50–60 % of the latent heat flux; moisture in the soil itself would have a reduced impact due to soil shading (Baldocchi et al., 2000). Another study found that the fraction of radiation that reaches

GMDD
7, 8649–8701, 2014

the soil ranges from 0.05 (forest) to 0.12 (tundra) (Beringer et al., 2005). The same study found that the latent heat flux correlates most closely with the leaf-level vapour pressure deficit – that is to say the difference between the leaf level saturation vapour pressure and the actual vapour pressure of the outside air, rather than between air water vapour pressure and the saturation vapour pressure at the soil level. Since a single layer canopy model regards both the canopy and soil surface as the same entity, the aforementioned subtleties will inevitably be lost in the modelling. Although, the partition of energy between soil surface and vegetation is site dependent – a well hydrated site would behave differently to one in an arid region – it is effects such as these that a more realistic energy budget scheme would be able to simulate.

Being able to simulate separately the vegetation allows for the partitioning of fluxes between the vegetation and the soil. For example, from the measurements (Fig. 8a and b), we see that approximately 70 % of the sensible heat that is measured above the canopy is sourced not from the soil surface, but from the overlying vegetation, as this is the difference between the measured flux at 1 m and that above the canopy. This is confirmed by the modelling results. There is no equivalent measurement at 1 m for the latent heat flux, but the model calculates that approximately 50 % of the latent heat flux is sourced from the vegetation rather than the soil surface.

This model also simulates leaf temperature that may be verified by leaf level measurements, where such measurements exist (Helliker and Richter, 2008). Such a comparison would require additional developments (as is discussed in the following section) because leaf temperature measurements strongly depend on the approach that is used.

7 Outlook

This document lays out the framework for the model design, but it allows for the further implementation of many features in site-level to global-scale scenarios:

GMDD
7, 8649–8701, 2014

– as the method calculates leaf temperature and in-canopy radiation, it will be possible to simulate the explicit emission by leaves of certain common Biogenic Volatile Organic Compounds (BVOCs), such as isoprene and monoterpene (Guenther et al., 1995, 2006). As the method calculates in-canopy gradients of temperature, specific humidity and radiation, it is possible to simulate more accurately chemical reactions that depend on these factors such as the NO_x and O_3 cycle within and above canopies (Walton et al., 1997) and the formation and size distribution of aerosol interactions (Atkinson and Arey, 2003; Nemitz et al., 2004a, b; Ehn et al., 2014), which may act as cloud condensation nuclei and thus again feedback into radiation absorption interactions at the atmospheric component of a coupled model such as LMDz/ORCHIDEE.

– Separate computation of vegetation and soil temperatures, which can be very different, and then to estimate accurate estimation of the whole canopy temperature and its directional effects. It may then be possible to assimilate this variable (which can also be measured from remote sensing) in order to better constrain the energy budget.

– Recent research in ecology demonstrates further the need to better understand canopy microclimates, and in particular gradients of state variables such as temperature and specific humidity, and radiation penetration. For example, temperature gradients in the rainforest exert a key influence on the habitat choices of frogs, and changes to such a microclimate threaten their survival (Scheffers et al., 2013). In a similar vein, microclimate affects in canopies can act as a buffer to changes in the climate overall (i.e. the macroclimate) in terms of the survival of species in the sub-canopy (Defraeye et al., 2014). Therefore structural forest changes, such as forest thinning, will reduce buffer lag effect, but it is only with well-designed canopy models that an informed prediction of the long term consequences of land management policies can be made.

GMDD
7, 8649–8701, 2014

8 Conclusions

A new numerical model for ORCHIDEE-CAN has been developed that enables the simulation of vertical canopy profiles of temperature and moisture using a non-iterative implicit scheme. This means that the new model may also be used when coupled to an atmospheric model, without compromising computer run-time. Initial tests demonstrated that the model runs stably, balances the energy budget at all levels, and provides a good simulation of the measured field data, both on short timescales of a few days, and over the course of a year. However, the model structure allows coupling/linking to a more physical-based albedo scheme (Pinty et al., 2006; McGrath et al., 2014; Naudts et al., 2014) and implementing a vertically discretised stomatal conductance scheme which both offer scope for improvement in model performance. The multi-layer energy budget model component outlined here may be used to simulate canopies in more detail and variety. It also offers the potential to integrate with other parts of ORCHIDEE for enhanced simulation of CO_2 transport, emission of VOCs and leaf scale plant hydraulics.

The Supplement related to this article is available online at doi:10.5194/gmdd-7-8649-2014-supplement.

Author contributions. J. Ryder and J. Polcher developed the numerical scheme. J. Ryder, J. Polcher, C. Ottlé, P. Peylin and S. Luyssaert designed the study and J. Ryder and S. Luyssaert wrote the manuscript with contributions from all co-authors. Y. Chen, M. J. McGrath, J. Otto, K. Naudts, S. Luyssaert and A. Valade helped J. Ryder with integrating the multi-layer energy budget model within ORCHIDEE-CAN. E. van Gorsel and V. Haverd provided field observations for the Tumbarumba site.

GMDD
7, 8649–8701, 2014

Acknowledgements. J. Ryder, Y. Chen, M. J. McGrath, J. Otto, K. Naudts and S. Luyssaert were funded through ERC starting grant 242564 (DOFOCO), and A. Valade was funded through ADEME (BiCaFF). ESA CCI Landcover also supported this work. The study benefited from an STSM (COST, TERRABITES ES0805) offered to J. Ryder. The authors would like to thank Aaron Boone for sharing his numerical scheme of an implicit coupling of snowpack and atmosphere temperature. Plots were produced using matplotlib (Hunter, 2007).

References

Atkinson, R. and Arey, J.: Gas-phase tropospheric chemistry of biogenic volatile organic compounds: a review, Atmos. Environ., 37, 197–219, doi:10.1016/S1352-2310(03)00391-1, 2003. 8679

Baldocchi, D. D.: A multi-layer model for estimating sulfur dioxide deposition to a deciduous oak forest canopy, Atmos. Environ., 22, 869–884, doi:10.1016/0004-6981(88)90264-8, 1988. 8655, 8659

Baldocchi, D. D. and Wilson, K.: Modeling CO_2 and water vapor exchange of a temperate broadleaved forest across hourly to decadal time scales, Ecol. Modell., 142, 155–184, doi:10.1016/S0304-3800(01)00287-3, 2001. 8653, 8654

Baldocchi, D. D., Law, B. E., and Anthoni, P. M.: On measuring and modeling energy fluxes above the floor of a homogeneous and heterogeneous conifer forest, Agr. Forest Meteorol., 102, 187–206, doi:10.1016/S0168-1923(00)00098-8, 2000. 8677

Baldocchi, D. D., Falge, E., Gu, L., Olson, R., Hollinger, D. Y., Running, S., Anthoni, P., Bernhofer, C., Davis, K., and Evans, R.: FLUXNET: a new tool to study the temporal and spatial variability of ecosystem-scale carbon dioxide, water vapor, and energy flux densities, B. Am. Meteorol. Soc., 82, 2415–2434, 2001. 8669

Ball, J. T., Woodrow, T., and Berry, J.: A model predicting stomatal conductance and its contribution to the control of photosynthesis under different environmental conditions, in: Proc. 7th Int. Congr. Photosynth., 221–224, 1987. 8654, 8671

Balsamo, G., Beljaars, A., Scipal, K., Viterbo, P., van den Hurk, B., Hirschi, M., and Betts, A. K.: A revised hydrology for the ECMWF model: verification from field site to terrestrial water storage and impact in the integrated forecast system, J. Hydrometeorol., 10, 623–643, doi:10.1175/2008JHM1068.1, 2009. 8652

GMDD

7, 8649–8701, 2014

Beringer, J., Chapin, F. S., Thompson, C. C., and Mcguire, A. D.: Surface energy exchanges along a tundra-forest transition and feedbacks to climate, Agr. Forest Meteorol., 131, 143–161, doi:10.1016/j.agrformet.2005.05.006, 2005. 8676, 8678

Best, M. J., Beljaars, A. C. M., Polcher, J., and Viterbo, P.: A proposed structure for coupling tiled surfaces with the planetary boundary layer, J. Hydrometeorol., 5, 1271–1278, 2004. 8655, 8668, 8675

Bonan, G. B.: Forests and climate change: forcings, feedbacks, and the climate benefits of forests, Science, 80, 320, 1444–1449, doi:10.1126/science.1155121, 2008. 8650

Bonan, G. B., Williams, M., Fisher, R. A., and Oleson, K. W.: Modeling stomatal conductance in the earth system: linking leaf water-use efficiency and water transport along the soil–plant–atmosphere continuum, Geosci. Model Dev., 7, 2193–2222, doi:10.5194/gmd-7-2193-2014, 2014. 8653

Chen, J., Menges, C., and Leblanc, S.: Global mapping of foliage clumping index using multi-angular satellite data, Remote Sens. Environ., 97, 447–457, doi:10.1016/j.rse.2005.05.003, 2005. 8691

de Noblet-Ducoudré, N., Boisier, J.-P., Pitman, A., Bonan, G. B., Brovkin, V., Cruz, F., Delire, C., Gayler, V., van den Hurk, B. J. J. M., Lawrence, P. J., van der Molen, M. K., Müller, C., Reick, C. H., Strengers, B. J., and Voldoire, A.: Determining robust impacts of land-use-induced land cover changes on surface climate over North America and Eurasia: results from the first set of LUCID experiments, J. Climate, 25, 3261–3281, doi:10.1175/JCLI-D-11-00338.1, 2012. 8652

Defraeye, T., Derome, D., Verboven, P., Carmeliet, J., and Nicolai, B.: Cross-scale modelling of transpiration from stomata via the leaf boundary layer, Ann. Bot., 114, 711–723, doi:10.1093/aob/mct313, 2014. 8679

Dobos, E.: Albedo, in: Encycl. Soil Sci., 2nd Edn., edited by: Lal, R., CRC Press, Chicago , USA, 64–66, doi:10.1201/NOE0849338304.ch15, 2005. 8691

Dolman, A. J.: A multiple-source land surface energy balance model for use in general circulation models, Agr. Forest Meteorol., 65, 21–45, doi:10.1016/0168-1923(93)90036-H, 1993. 8653, 8654, 8674, 8676

Dolman, A. J. and Wallace, J.: Lagrangian and K-theory approaches in modelling evaporation from sparse canopies, Q. J. Roy. Meteor. Soc., 117, 1325–1340, 1991. 8677

Ehn, M., Thornton, J. A., Kleist, E., Sipilä, M., Junninen, H., Pullinen, I., Springer, M., Rubach, F., Tillmann, R., Lee, B., Lopez-Hilfiker, F., Andres, S., Acir, I.-H., Rissanen, M.,

GMDD
7, 8649–8701, 2014

Jokinen, T., Schobesberger, S., Kangasluoma, J., Kontkanen, J., Nieminen, T., Kurtén, T., Nielsen, L. B., Jø rgensen, S., Kjaergaard, H. G., Canagaratna, M., Maso, M. D., Berndt, T., Petäjä, T., Wahner, A., Kerminen, V.-M., Kulmala, M., Worsnop, D. R., Wildt, J., and Mentel, T. F.: A large source of low-volatility secondary organic aerosol., Nature, 506, 476–479, doi:10.1038/nature13032, 2014. 8679

Gao, W., Shaw, R. H., and Paw, K. T.: Observation of organized structure in turbulent flow within and above a forest canopy, Bound.-Lay. Meteorol., 47, 349–377, 1989. 8677

Gu, L.: Longwave radiative transfer in plant canopies, Ph.D. thesis, University of Virginia, Charlottesville, Virginia, USA, 1988. 8669

Gu, L., Shugart, H. H., Fuentes, J. D., Black, T. A., and Shewchuk, S. R.: Micrometeorology, biophysical exchanges and NEE decomposition in a two-storey boreal forest – development and test of an integrated model, Agr. Forest Meteorol., 94, 123–148, 1999. 8669

Guenther, A., Karl, T., Harley, P., Wiedinmyer, C., Palmer, P. I., and Geron, C.: Estimates of global terrestrial isoprene emissions using MEGAN (Model of Emissions of Gases and Aerosols from Nature), Atmos. Chem. Phys., 6, 3181–3210, doi:10.5194/acp-6-3181-2006, 2006. 8679

Guenther, A. B., Nicholas, C., Fall, R., Klinger, L., Mckay, W. A., and Scholes, B.: A global model of natural volatile organic compound emissions, J. Geophys. Res., 100, 8873–8892, 1995. 8679

Haverd, V., Leuning, R., Griffith, D., Gorsel, E., and Cuntz, M.: The turbulent Lagrangian time scale in forest canopies constrained by fluxes, concentrations and source distributions, Bound.-Lay. Meteorol., 130, 209–228, doi:10.1007/s10546-008-9344-4, 2009. 8670

Helliker, B. R. and Richter, S. L.: Subtropical to boreal convergence of tree-leaf temperatures, Nature, 454, 511–514, doi:10.1038/nature07031, 2008. 8678

Hourdin, F., Musat, I., Bony, S., Braconnot, P., Codron, F., Dufresne, J.-L., Fairhead, L., Filiberti, M.-A., Friedlingstein, P., Grandpeix, J.-Y., Krinner, G., LeVan, P., Li, Z.-X., and Lott, F.: The LMDZ4 general circulation model: climate performance and sensitivity to parametrized physics with emphasis on tropical convection, Clim. Dynam., 27, 787–813, doi:10.1007/s00382-006-0158-0, 2006. 8655

Hunter, J. D.: Matplotlib: a 2D graphics environment, Comput. Sci. Eng., 9, 90–95, 2007. 8681

Jacobson, M. Z.: Fundamentals of Atmospheric Modeling, 2nd Edn., Cambridge University Press, New York, 2005. 8661

GMDD
7, 8649–8701, 2014

Jarvis, P.: The interpretation of the variations in leaf water potential and stomatal conductance found in canopies in the fields, Philos. Trans. R. Soc. London, Ser. B, 593–610, 1976. 8659, 8671

Jiménez, C., Prigent, C., Mueller, B., Seneviratne, S. I., McCabe, M. F., Wood, E. F., Rossow, W. B., Balsamo, G., Betts, A. K., Dirmeyer, P. A., Fisher, J. B., Jung, M., Kanamitsu, M., Reichle, R. H., Reichstein, M., Rodell, M., Sheffield, J., Tu, K., and Wang, K.: Global intercomparison of 12 land surface heat flux estimates, J. Geophys. Res., 116, D02102, doi:10.1029/2010JD014545, 2011. 8652

Krinner, G., Viovy, N., de Noblet-Ducoudré, N., Ogee, J., Polcher, J., Friedlingstein, P., Ciais, P., Sitch, S., and Prentice, I. C.: A dynamic global vegetation model for studies of the coupled atmosphere–biosphere system, Global Biogeochem. Cy., 19, 1–33, doi:10.1029/2003GB002199, 2005. 8651

Lohammer, T., Larsson, S., Linder, S., and Falk, S. O.: Simulation models of gaseous exchange in Scotch pine. Structure and function of Northern Coniferous Forest, Ecol. Bull., 32, 505–523, 1980. 8659

Lovell, J., Haverd, V., Jupp, D., and Newnham, G.: The Canopy Semi-analytic Pgap And Radiative Transfer (CanSPART) model: Validation using ground based lidar, Agr. Forest Meteorol., 158–159, 1–12, doi:10.1016/j.agrformet.2012.01.020, 2012. 8671

LSCE/IPSL: ORCHIDEE documentation, available at: http://dods.ipsl.jussieu.fr/orchidee/DOXYGEN/webdoc/ (last access: 2 December 2014), 2012. 8676

Makar, P. A., Fuentes, J. D., Wang, D., Staebler, R. M., and Wiebe, H. A.: Chemical processing of biogenic hydrocarbons within and above a temperate deciduous forest, J. Geophys. Res., 104, 3581–3603, doi:10.1029/1998JD100065, 1999. 8662, 8677, 8691

Martens, S. N., Ustin, S. L., and Rousseau, R. A.: Estimation of tree canopy leaf area index by gap fraction analysis, Forest Ecol. Manag., 61, 91–108, 1993. 8691

Massman, W. J. and Weil, J. C.: An analytical one-dimensional second-order closure model of turbulence statistics and the lagrangian time scale within and above plant canopies of arbitrary structure, Bound.-Lay. Meteorol., 91, 81–107, 1999. 8661, 8677

McGrath, M. J., Pinty, B., Ryder, J., Otto, J., and Luyssaert, S.: A multilevel canopy radiative transfer scheme based on a domain-averaged structure factor, in preparation, 2014. 8654, 8680

GMDD
7, 8649–8701, 2014

McNaughton, K. G. and van den Hurk, B. J. J. M.: A "Lagrangian" revision of the resistors in the two-layer model for calculating the energy budget of a plant canopy, Bound.-Lay. Meteorol., 74, 261–288, 1995. 8662, 8677

Medlyn, B. E., Duursma, R. A., Eamus, D., Ellsworth, D. S., Prentice, I. C., Barton, C. V. M., Crous, K. Y., De Angelis, P., Freeman, M., and Wingate, L.: Reconciling the optimal and empirical approaches to modelling stomatal conductance, Glob. Change Biol., 17, 2134–2144, doi:10.1111/j.1365-2486.2010.02375.x, 2011. 8654, 8659

Monteith, J. and Unsworth, M. H.: Principles of Environmental Physics, Academic Press (Elsevier), Waltham, Massachusetts, USA, 2008. 8656, 8657, 8658

Naudts, K., Ryder, J., J. McGrath, M., Otto, J., Chen, Y., Valade, A., Bellasen, V., Berhongaray, G., Bönisch, G., Campioli, M., Ghattas, J., De Groote, T., Haverd, V., Kattge, J., MacBean, N., Maignan, F., Merilä, P., Penuelas, J., Peylin, P., Pinty, B., Pretzsch, H., Schulze, E. D., Solyga, D., Vuichard, N., Yan, Y., and Luyssaert, S.: A vertically discretised canopy description for ORCHIDEE (SVN r2290) and the modifications to the energy, water and carbon fluxes, Geosci. Model Dev. Discuss., 7, 8565–8647, doi:10.5194/gmdd-7-8565-2014, 2014. 8651, 8671, 8680

Nemitz, E., Sutton, M. A., Wyers, G. P., and Jongejan, P. A. C.: Gas-particle interactions above a Dutch heathland: I. Surface exchange fluxes of NH_3, SO_2, HNO_3 and HCl, Atmos. Chem. Phys., 4, 989–1005, doi:10.5194/acp-4-989-2004, 2004a. 8679

Nemitz, E., Sutton, M. A., Wyers, G. P., Otjes, R. P., Mennen, M. G., van Putten, E. M., and Gallagher, M. W.: Gas-particle interactions above a Dutch heathland: II. Concentrations and surface exchange fluxes of atmospheric particles, Atmos. Chem. Phys., 4, 1007–1024, doi:10.5194/acp-4-1007-2004, 2004b. 8679

Nobel, P.: Physiochemical and Environmental Plant Physiology, 3rd Edn., Academic Press (Elsevier), Waltham, Massachusetts, USA, 2005. 8691

Ogée, J., Brunet, Y., Loustau, D., Berbigier, P., and Delzon, S.: MuSICA, a CO_2, water and energy multilayer, multileaf pine forest model: evaluation from hourly to yearly time scales and sensitivity analysis, Glob. Change Biol., 9, 697–717, doi:10.1046/j.1365-2486.2003.00628.x, 2003. 8653, 8655, 8691

Ozflux: Description of Tumbarumba monitoring station, available at: www.ozflux.org.au/monitoringsites/tumbarumba (last access: 2 December 2014), 2013. 8669, 8671

GMDD
7, 8649–8701, 2014

Park, G.-H., Gao, X., and Sorooshian, S.: Estimation of surface longwave radiation components from ground-based historical net radiation and weather data, J. Geophys. Res., 113, D04207, doi:10.1029/2007JD008903, 2008. 8670

Penman, H. L. and Schofield, R. K.: Some physical aspects of assimilation and transpiration, Symp. Soc. Exp. Biol., 5, 115–129, 1951. 8653

Pinty, B., Lavergne, T., Dickinson, R. E., Widlowski, J.-L., Gobron, N., and Verstraete, M. M.: Simplifying the interaction of land surfaces with radiation for relating remote sensing products to climate models, J. Geophys. Res., 111, 1–20, doi:10.1029/2005JD005952, 2006. 8654, 8680

Pitman, A. J., de Noblet-Ducoudré, N., Cruz, F. T., Davin, E. L., Bonan, G. B., Brovkin, V., Claussen, M., Delire, C., Ganzeveld, L., Gayler, V., van den Hurk, B. J. J. M., Lawrence, P. J., van der Molen, M. K., Müller, C., Reick, C. H., Seneviratne, S. I., Strengers, B. J., and Voldoire, A.: Uncertainties in climate responses to past land cover change: First results from the LUCID intercomparison study, Geophys. Res. Lett., 36, L14814, doi:10.1029/2009GL039076, 2009. 8652

Polcher, J., McAvaney, B., Viterbo, P., Gaertner, M., Hahmann, A., Mahfouf, J.-F., Noilhan, J., Phillips, T., Pitman, A. J., Schlosser, C., Schulz, J.-P., Timbal, B., Verseghy, D. L., and Xue, Y.: A proposal for a general interface between land surface schemes and general circulation models, Glob. Planet. Change, 19, 261–276, 1998. 8655, 8656, 8675

Raupach, M. R.: Applying Lagrangian fluid mechanics to infer scalar source distributions from concentration profiles in plant canopies, Agr. Forest Meteorol., 47, 85–108, 1989a. 8662, 8677

Raupach, M. R.: A practical Lagrangian method for relating scalar concentrations to source distributions in vegetation canopies, Q. J. Roy. Meteor. Soc., 115, 609–632, doi:10.1256/smsqj.48709, 1989b. 8662, 8677

Richtmyer, R. D. and Morton, K. W.: Difference Methods for Initial-Value Problems, 2nd Edn., Wiley-Interscience, New York, USA, 1967. 8664, 8666

Saux-Picart, S., Ottlé, C., Perrier, a., Decharme, B., Coudert, B., Zribi, M., Boulain, N., Cappelaere, B., and Ramier, D.: SEtHyS_Savannah: a multiple source land surface model applied to Sahelian landscapes, Agr. Forest Meteorol., 149, 1421–1432, doi:10.1016/j.agrformet.2009.03.013, 2009. 8653, 8654

GMDD
7, 8649–8701, 2014

Scheffers, B. R., Phillips, B. L., Laurance, W. F., Sodhi, N. S., Diesmos, A., Williams, E., and Williams, S. E.: Increasing arboreality with altitude: a novel biogeographic dimension, Proc. R. Soc. B, 280, 1–9, doi:10.1098/rspb.2013.1581, 2013. 8679

Schlosser, C. A. and Gao, X.: Assessing evapotranspiration estimates from the second Global Soil Wetness Project (GSWP-2) simulations, J. Hydrometeorol., 11, 880–897, doi:10.1175/2010JHM1203.1, 2010. 8652

Schulz, J.-P., Dümenil, L., and Polcher, J.: On the land surface–atmosphere coupling and its impact in a single-column atmospheric model, J. Appl. Meteorol., 40, 642–663, doi:10.1175/1520-0450(2001)040<0642:OTLSAC>2.0.CO;2, 2001. 8651

Seneviratne, S. I., Corti, T., Davin, E. L., Hirschi, M., Jaeger, E. B., Lehner, I., Orlowsky, B., and Teuling, A. J.: Investigating soil moisture–climate interactions in a changing climate: a review, Earth-Science Rev., 99, 125–161, doi:10.1016/j.earscirev.2010.02.004, 2010. 8652

Shuttleworth, W. J. and Wallace, J. S.: Evaporation from sparse crops – an energy combination theory, Q. J. Roy. Meteor. Soc., 111, 839–855, doi:10.1256/smsqj.46909, 1985. 8653

Singles, R., Sutton, M., and Weston, K.: A multi-layer model to describe the atmospheric transport and deposition of ammonia in Great Britain, Atmos. Environ., 32, 393–399, doi:10.1016/S1352-2310(97)83467-X, 1998. 8661

Sinoquet, H., Le Roux, X., Adam, B., Ameglio, T., and Daudet, F. A.: RATP: a model for simulating the spatial distribution of radiation absorption, transpiration and photosynthesis within canopies: application to an isolated tree crown, Plant, Cell Environ., 24, 395–406, doi:10.1046/j.1365-3040.2001.00694.x, 2001. 8654

Stroud, C., Makar, P. A., Karl, T., Guenther, A. B., Geron, C., Turnipseed, A., Nemitz, E. G., Baker, B., Potosnak, M. J., and Fuentes, J. D.: Role of canopy-scale photochemistry in modifying biogenic-atmosphere exchange of reactive terpene species: Results from the CELTIC field study, J. Geophys. Res., 110, 1–14, doi:10.1029/2005JD005775, 2005. 8662, 8677

Verhoef, A. and Allen, S. J.: A SVAT scheme describing energy and CO2 fluxes for multi-component vegetation: calibration and test for a Sahelian savannah, Ecol. Modell., 127, 245–267, doi:10.1016/S0304-3800(99)00213-6, 2000. 8653, 8654

Vieno, M.: The use of an atmospheric chemistry-transport model (FRAME) over the UK and the development of its numerical and physical schemes, Ph.D. thesis, University of Edinburgh, Edinburgh, UK, 2006. 8661

GMDD
7, 8649–8701, 2014

Vuichard, N. and Papale, D.: Filling the gaps in meteorological continuous data measured at Fluxnet sites with ERA-interim reanalysis, Earth Syst. Sci. Data Discuss., submitted, 2014. 8671

Waggoner, P. E., Furnival, G. M., and Reifsnyder, W. E.: Simulation of the microclimate in a forest, For. Sci., 15, 37–45, 1969. 8656

Walton, S., Gallagher, M. W., and Duyzer, J. H.: Use of a detailed model to study the exchange of NOx and O3 above and below a deciduous canopy, Atmos. Environ., 31, 2915–2931, doi:10.1016/S1352-2310(97)00126-X, 1997. 8679

Wilson, K., Goldstein, A. H., Falge, E., Aubinet, M., Baldocchi, D. D., Berbigier, P., Bernhofer, C., Ceulemans, R., Dolman, H., Field, C., Grelle, A., Ibrom, A., Law, B., Kowalski, A., Meyers, T., Moncrieff, J. B., Monson, R. K., Oechel, W., Tenhunen, J., Valentini, R., and Verma, S.: Energy balance closure at FLUXNET sites, Agr. Forest Meteorol., 113, 223–243, doi:10.1016/S0168-1923(02)00109-0, 2002. 8672

Wolfe, G. M. and Thornton, J. A.: The Chemistry of Atmosphere-Forest Exchange (CAFE) Model – Part 1: Model description and characterization, Atmos. Chem. Phys., 11, 77–101, doi:10.5194/acp-11-77-2011, 2011. 8662, 8677

Yamazaki, T., Kondo, J., and Watanabe, T.: A heat-balance model with a canopy of one or two layers and its application to field experiments, J. Appl. Meteorol., 31, 86–103, 1992. 8653, 8691

Zhao, W. and Qualls, R. J.: A multiple-layer canopy scattering model to simulate shortwave radiation distribution within a homogeneous plant canopy, Water Resour. Res., 41, 1–16, doi:10.1029/2005WR004016, 2005. 8653

Zhao, W. and Qualls, R. J.: Modeling of long-wave and net radiation energy distribution within a homogeneous plant canopy via multiple scattering processes, Water Resour. Res., 42, 1–13, doi:10.1029/2005WR004581, 2006. 8653

GMDD
7, 8649–8701, 2014

Table 1. Notation list.

Symbol	Description
T^t, T^{t+1}	Temperature at the "present" and "next" timestep respectively (K)
q^t, q^{t+1}	Specific humidity at the "present" and "next" timestep ($\mathrm{kg\,kg^{-1}}$)
T_i^{L}	Leaf temperature at level "i" (K)
q_i^{L}	Leaf specific humidity at level "i" ($\mathrm{kg\,kg^{-1}}$)
T_i^{a}	Atmospheric temperature at level "i" (K)
q_i^{a}	Atmospheric specific humidity at level "i" ($\mathrm{kg\,kg^{-1}}$)
ΔT	Interval between "present" and "next" timestep (s)
Δz_i	Difference in height between potential at level "i" and level "$i+1$" (m)
Δh_i	Thickness of level "i" (m)
ϵ_i	Emissivity fraction at level "i" (–)
ω_i	Leaf interception coefficient at level "i" (–)
$K_{\mathrm{LW}}, K_{\mathrm{SW}}$	Canopy extinction coefficient for longwave and shortwave, respectively (–)
ρ_i^{alb}	Albedo of vegetation layer "i" (–)
λ	Latent heat of vapourisation ($\mathrm{J\,kg^{-1}}$)
$\rho_{\mathrm{v}}, \rho_{\mathrm{a}}$	Vegetation and atmospheric density, respectively ($\mathrm{kg\,m^{-3}}$)
σ	Stefan–Boltzmann constant ($5.67 \times 10^{-8}\,\mathrm{W\,m^{-2}\,K^{-4}}$)
θ_i	Leaf layer heat capacity at level "i" ($\mathrm{J\,(kg\,K)^{-1}}$)
$\Theta_{p,\,\mathrm{a}}$	Specific heat capacity of air ($\mathrm{J\,(kg\,K)^{-1}}$)
R_i, R_i'	Stomatal resistance at level "i" for sensible and latent heat flux, respectively ($\mathrm{s\,m^{-1}}$)
LE_i, H_i	Latent heat and sensible heat flux at level "i", respectively ($\mathrm{W\,m^{-2}}$)
$\mathrm{LE}_{\mathrm{tot}}, H_{\mathrm{tot}}$	Total latent heat and sensible heat flux at canopy top, respectively ($\mathrm{W\,m^{-2}}$)
$R_{\mathrm{LW},i}, R_{\mathrm{SW},i}$	Long-wave and short wave radiation received by level "i", respectively ($\mathrm{W\,m^{-2}}$)
k_i	Diffusivity coefficient for level "i" ($\mathrm{m^2\,s^{-1}}$)
$A_{T,i}, B_{T,i}, C_{T,i}, D_{T,i}$	Components for substituted Eq. (i)
$A_{q,i}, B_{q,i}, C_{q,i}, D_{q,i}$	Components for substituted Eq. (ii)
E_i, F_i, G_i	Components for substituted Eq. (iii)
θ_0	Heat capacity of the infinitesimal surface layer ($\mathrm{J\,(K\,m^2)^{-1}}$)
J_{soil}	Heat flux from the sub-soil ($\mathrm{W\,m^{-2}}$)
$\phi_H, \phi_{\mathrm{LE}}$	Respectively sensible and latent heat flux from the infinitesimal surface layer ($\mathrm{W\,m^{-2}}$)

GMDD
7, 8649–8701, 2014

Table 2. Input coefficients at the top layer of the model, where $A_{T,n}, B_{T,n} \ldots$ etc are the respective coefficients at the top of the surface model and $A_{T,\text{atmos}}$, $B_{T,\text{atmos}}$ are the coefficients at the lowest level of the atmospheric model.

Stand-alone model	Coupled model
$A_{T,n} = 0$	$A_{T,n} = A_{T,\text{atmos}}$
$B_{T,n} = B_{T,\text{input}}$	$B_{T,n} = B_{T,\text{atmos}}$
$C_{T,n} = 0$	$C_{T,n} = 0$
$D_{T,n} = 0$	$D_{T,n} = 0$
$A_{q,n} = 0$	$A_{q,n} = A_{q,\text{atmos}}$
$B_{q,n} = B_{q,\text{input}}$	$B_{q,n} = B_{q,\text{atmos}}$
$C_{q,n} = 0$	$C_{q,n} = 0$
$D_{q,n} = 0$	$D_{q,n} = 0$

GMDD
7, 8649–8701, 2014

Table 3. Tuning coefficients used in the model for simulation described in this work.

symbol (as here)	description	code ref.	initial value	tuned value(s)	reference example
number of levels	number of levels	nlvls	50	25, 10, 5, 2, 1	Yamazaki et al. (1992); Ogée et al. (2003)
$R(\tau)$	eddy diff. tuning coef.	k_eddy_fac	1.0	0.6 (day); 0.2 (night)	Makar et al. (1999)
m_{veg}	leaf mass	(leaf_tks * rho_veg)	0.21	0.14 kg m^{-2}	Nobel (2005), Sect. 7.1
Ω	canopy gap fraction	canopy_gap	1.0	0.4	Chen et al. (2005)
ρ_{albedo}	albedo	rho_albedo	0.2	0.1	Dobos (2005)
K_{SW}	SW extinction coefficient	bigk_sw	0.5	0.4	Martens et al. (1993)

GMDD
7, 8649–8701, 2014

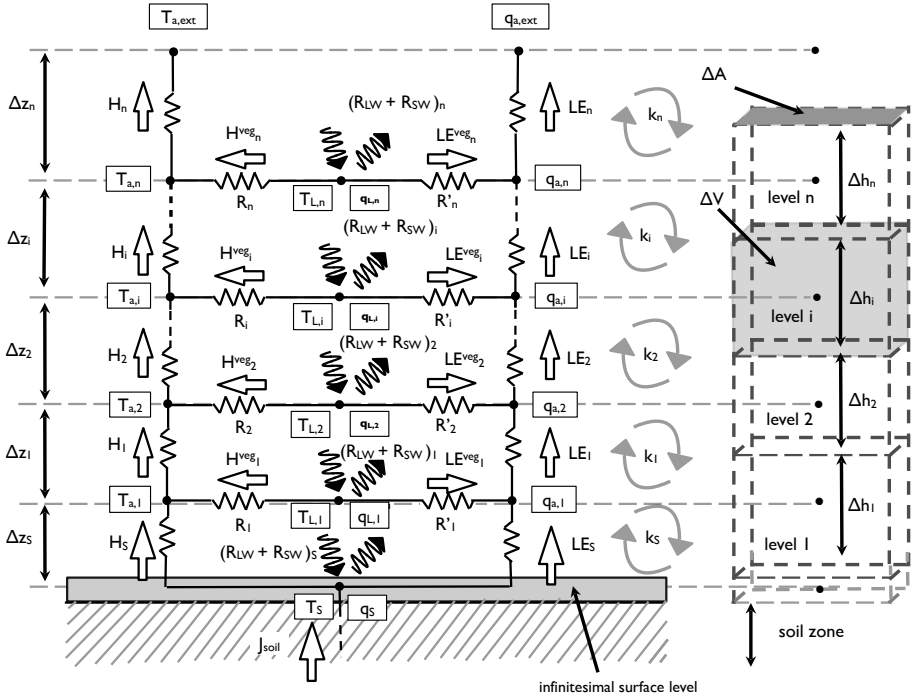

Figure 1. Resistance analogue for a multilayer canopy approximation of "*n*" levels, to which the energy balance applies at each level. Refer to Table 1 for the interpretation of symbols.

GMDD
7, 8649–8701, 2014

A multi-layer land surface energy budget model

J. Ryder et al.

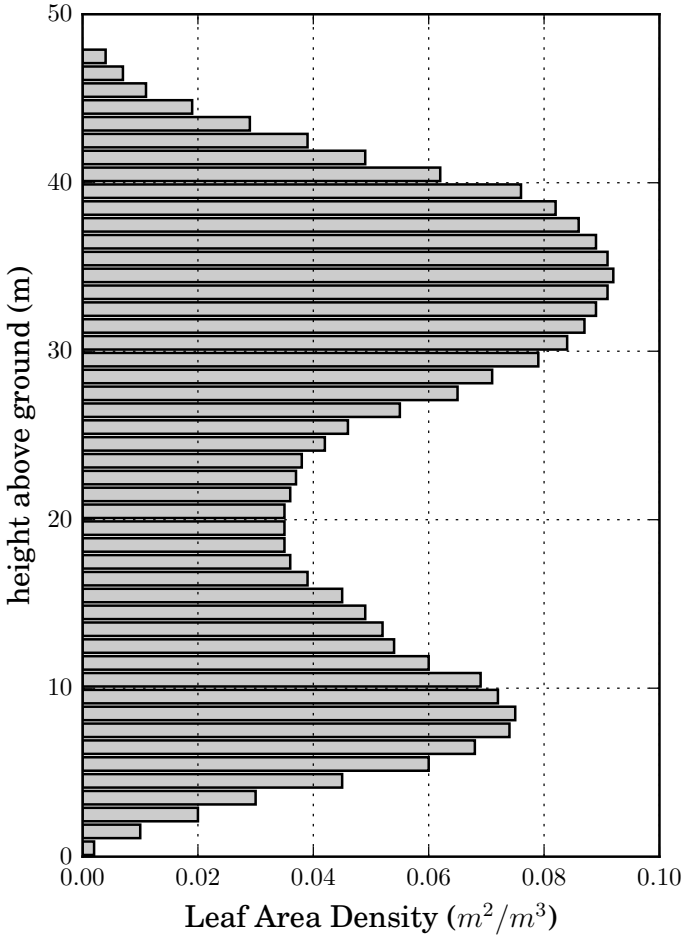

Figure 2. Imposed Leaf Area Density Profile for the forest canopy at TumbaTower used in this study.

GMDD
7, 8649–8701, 2014

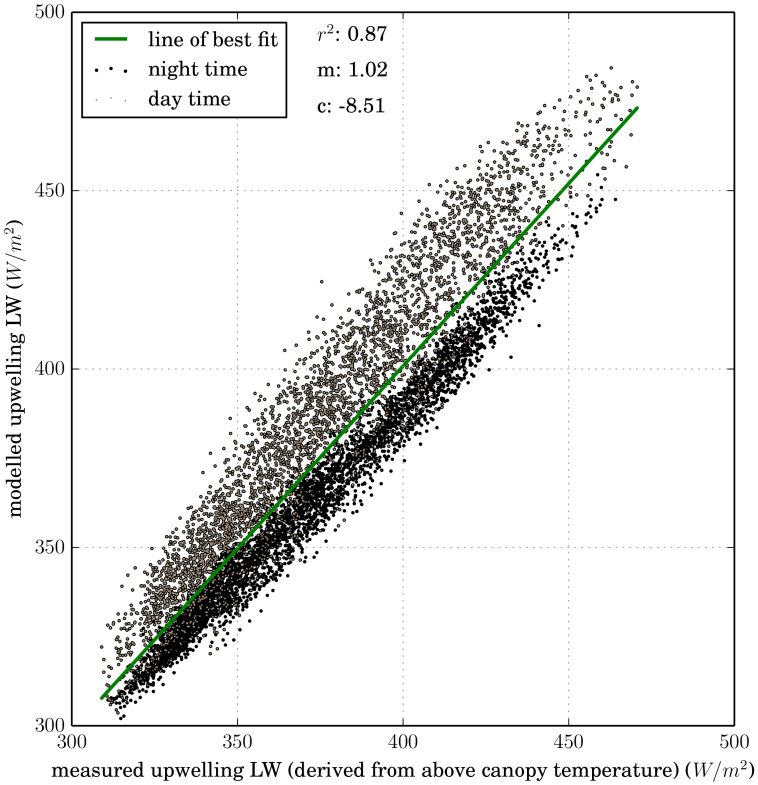

Figure 3. Correlation of observed upwelling longwave radiation (derived from the measured above-canopy temperature) and the upwelling longwave radiation that is simulated by the model. Nighttime data (corresponding to a downwelling shortwave radiation of $< 10\,W\,m^{-2}$) are plotted in black, and daytime data plotted in orange.

GMDD
7, 8649–8701, 2014

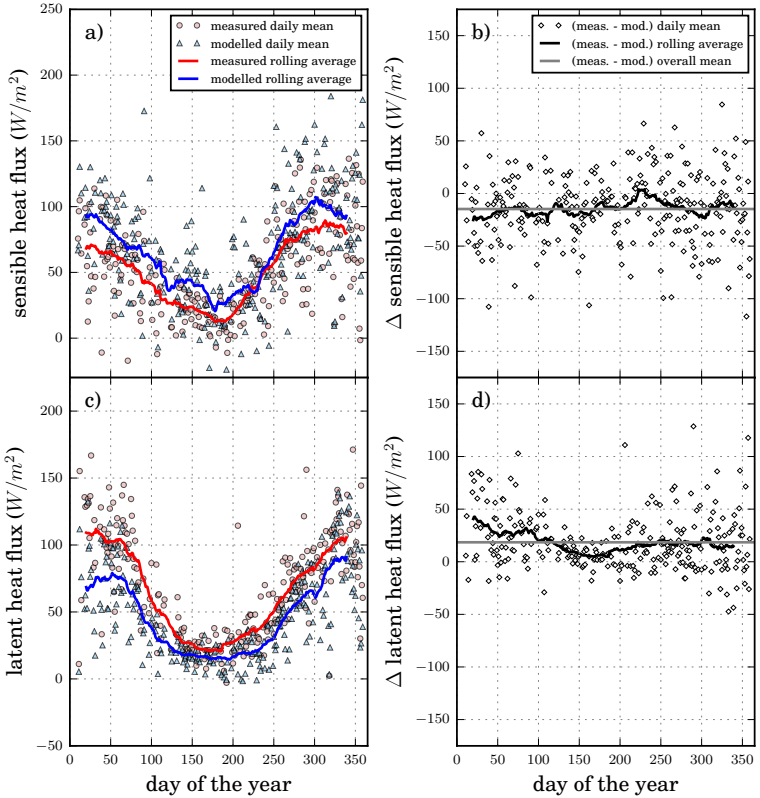

Figure 4. Daily mean for measured (circles) and modelled (triangles) over a year-long run for **(a)** sensible heat flux; **(b)** difference between measured and modelled sensible heat flux; **(c)** latent heat flux; and **(d)** difference between measured and modelled latent heat flux. One in every 5 data points is shown, for clarity. Thick lines show the respective 20 day rolling average respectively for each dataset. Graphs **(b)** and **(d)** also show the overall mean of individual data points.

GMDD
7, 8649–8701, 2014

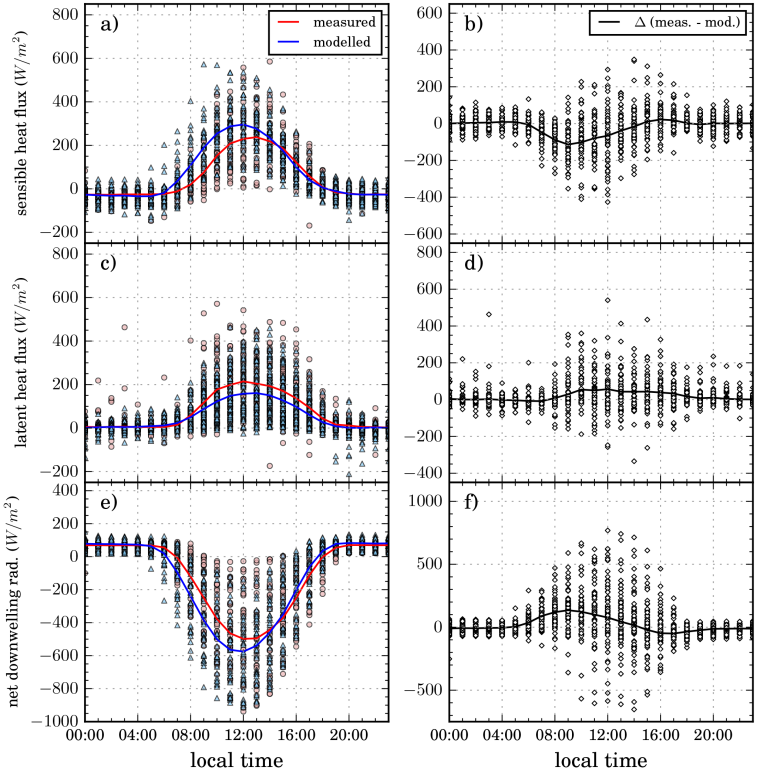

Figure 5. Hourly means for measured (circles) and modelled (triangles) for **(a)** measured and modelled sensible heat flux; **(b)** difference between measured and modelled sensible heat flux, as calculated over a two period of 2006 and 2007. One in every 10th day is plotted for clarity; **(c)** and **(d)**: as above for latent heat flux; **(e)** and **(f)**: as above for net radiation. Continuous lines show the overall mean.

GMDD
7, 8649–8701, 2014

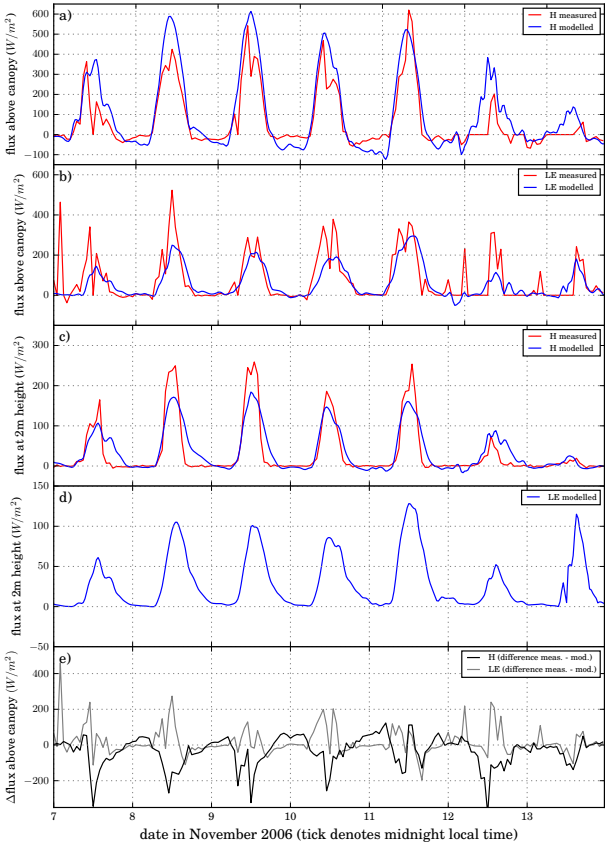

Figure 6. (a) measured and modelled sensible heat fluxes at a height of 50 m; **(b)** as **(a)** for latent heat flux; **(c)** measured and modelled sensible heat flux at 2 m above the ground; **(d)** modelled latent heat flux at 2 m above the ground (measurements not available); **(e)** difference in measured and modelled sensible and latent heat flux at a height of 50 m.

GMDD
7, 8649–8701, 2014

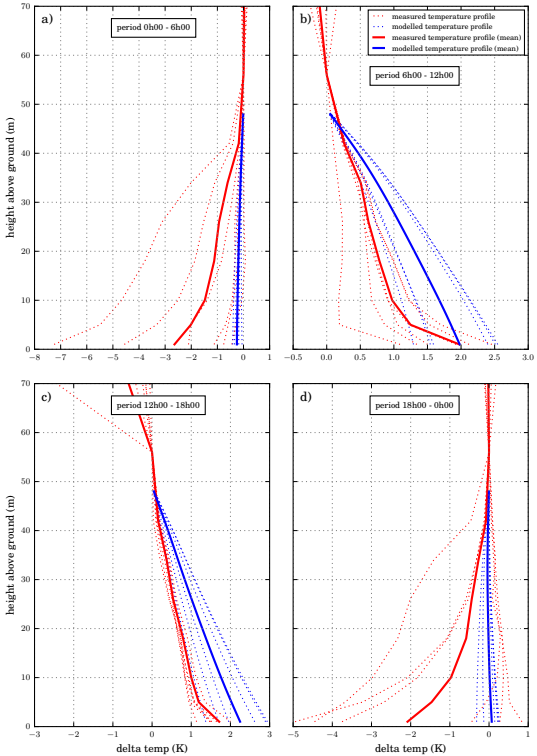

Figure 7. Model run with an eddy coefficient forcing factor of unity. Plots show the seven day (6 to 12 November 2006) mean modelled temperature gradients (bold in blue) within the canopy against the measured temperature gradients (bold in red) for the local time periods: **(a)** 00:00–06:00; **(b)** 06:00–12:00; **(c)** 12:00–18:00 and **(d)** 18:00–00:00, both expressed as a difference from the temperature at the top of canopy. Also shown are the measured and modelled data for each individual day, as dotted lines in the corresponding colour.

GMDD
7, 8649–8701, 2014

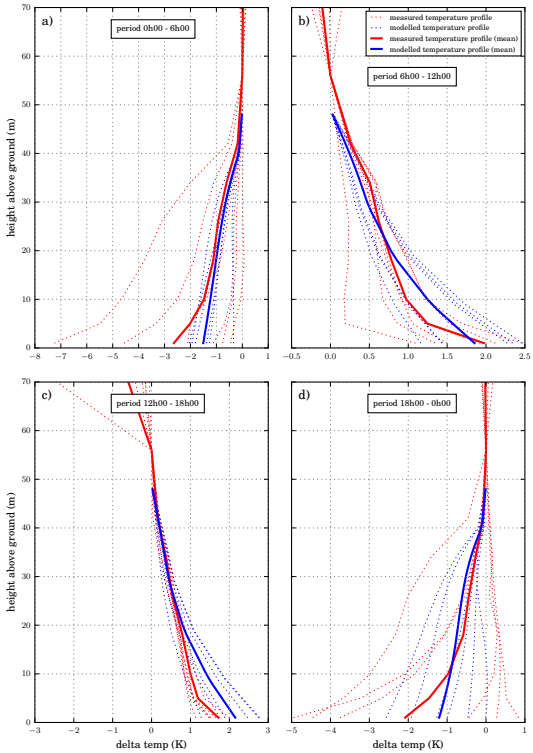

Figure 8. Model run with smaller eddy coefficient factor of 0.6 (daytime) and 0.2 (nightime) within the canopy. Plots show the seven day (6 to 12 November 2006) mean modelled temperature gradients (bold in blue) within the canopy against the measured temperature gradients (bold in red) for the local time periods: **(a)** 00:00–06:00; **(b)** 06:00–12:00; **(c)** 12:00–18:00 and **(d)** 18:00–00:00, both expressed as a difference from the temperature at top of canopy. Also shown are the measured and modelled data for each individual day, as dotted lines in the corresponding colour.

GMDD
7, 8649–8701, 2014

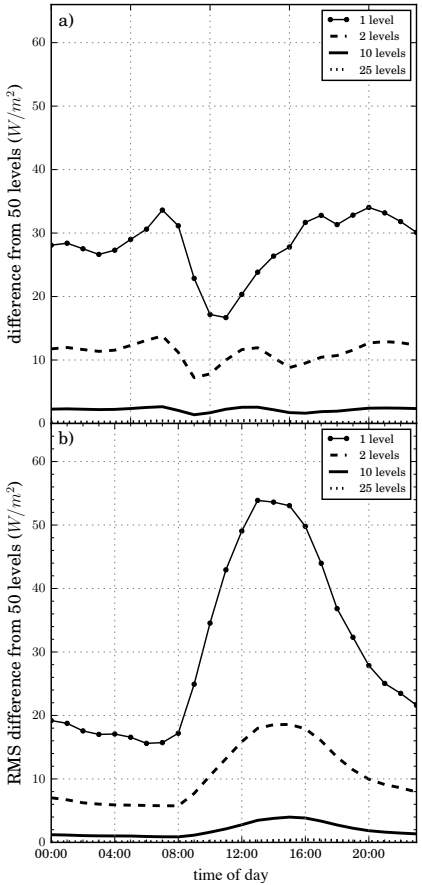

Figure 9. (a) Root mean square difference between 50 level hourly average simulation of sensible heat flux and modelled 25, 10, 2 and 1 level (plus the soil surface level) simulation of the same quantity; **(b)** as **(a)** for latent heat flux. Time shown is local time.

GMDD
7, 8649–8701, 2014

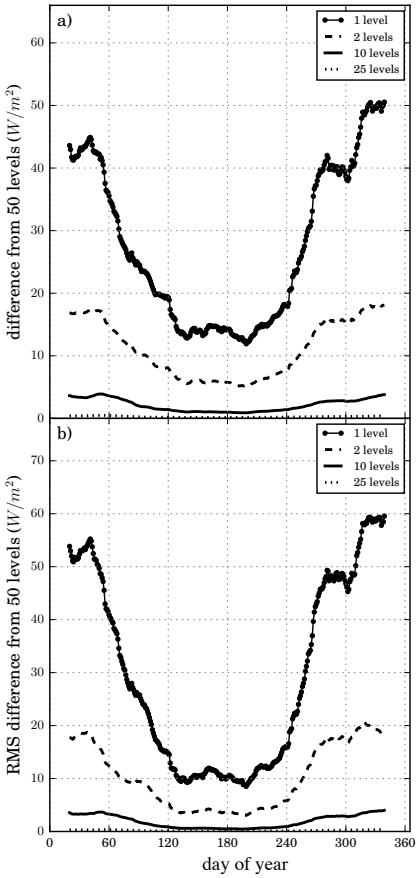

Figure 10. (a) 20 day rolling average of the root mean square difference of the daily mean, between the 50 level simulation of sensible heat flux and modelled 25, 10, 2 and 1 level (plus the soil surface level) simulation of the same quantity; **(b)** as **(a)** for latent heat flux. Time shown is local time.

GMDD
7, 8649–8701, 2014